

# Depth-resolved measurement of the Meissner screening profile in a niobium thin film from spin-lattice relaxation of the implanted $\beta$ -emitter $^8\text{Li}$

Ryan M. L. McFadden,<sup>1,2,a</sup> Md Asaduzzaman,<sup>1,2</sup> Terry J. Buck,<sup>3,b</sup> David L. Cortie,<sup>3,4,5,c</sup> Martin H. Dehn,<sup>3,5,d</sup> Sarah R. Dunsiger,<sup>1,6</sup> Robert F. Kiefl,<sup>1,3,5</sup> Robert E. Laxdal,<sup>1,2</sup> C. D. Philip Levy,<sup>1</sup> W. Andrew MacFarlane,<sup>1,4,5</sup> Gerald D. Morris,<sup>1</sup> Matthew R. Pearson,<sup>1,e</sup> Edward Thoeng,<sup>1,3</sup> and Tobias Junginger<sup>1,2,f</sup>

<sup>1</sup>TRIUMF, 4004 Wesbrook Mall, Vancouver, BC V6T 2A3, Canada

<sup>2</sup>Department of Physics and Astronomy, University of Victoria, 3800 Finnerty Road, Victoria, BC V8P 5C2, Canada

<sup>3</sup>Department of Physics and Astronomy, 6224 Agricultural Road, University of British Columbia, Vancouver, BC V6T 1Z1, Canada

<sup>4</sup>Department of Chemistry, 2036 Main Mall, University of British Columbia, Vancouver, BC V6T 1Z1, Canada

<sup>5</sup>Stewart Blusson Quantum Matter Institute, 2355 East Mall, University of British Columbia, Vancouver, BC V6T 1Z4, Canada

<sup>6</sup>Department of Physics, Simon Fraser University, 8888 University Drive, Burnaby, BC V5A 1S6, Canada

(Dated: 7 September 2023)

We report measurements of the Meissner screening profile in a Nb(300nm)/Al<sub>2</sub>O<sub>3</sub> thin film using  $^8\text{Li}$   $\beta$ -detected nuclear magnetic resonance ( $\beta$ -NMR). The NMR probe  $^8\text{Li}$  was ion-implanted into the Nb film at energies  $\leq 20$  keV, corresponding to mean stopping depths comparable to Nb's magnetic penetration depth  $\lambda$ .  $^8\text{Li}$ 's strong dipole-dipole coupling with the host  $^{93}\text{Nb}$  nuclei provided a “cross-relaxation” channel that dominated in low magnetic fields, which conferred indirect sensitivity to the local magnetic field via the spin-lattice relaxation (SLR) rate  $1/T_1$ . From a fit of the  $1/T_1$  data to a model accounting for its dependence on temperature, magnetic field, and  $^8\text{Li}^+$  implantation energy, we obtained a magnetic penetration depth  $\lambda_0 = 51.5(22)$  nm, consistent with a relatively short carrier mean-free-path  $\ell = 18.7(29)$  nm typical of similarly prepared Nb films. The results presented here constitute an important step towards using  $^8\text{Li}$   $\beta$ -NMR to characterize bulk Nb samples with engineered surfaces, which are often used in the fabrication of particle accelerators.

## I. INTRODUCTION

The transition metal Nb is a type-II superconductor with a transition temperature  $T_c \approx 9.25$  K<sup>1</sup> that is highest among the pure elements. Accompanying this accolade is the highest lower critical field  $B_{c1} \approx 170$  mT<sup>1</sup> of any known superconductor, making Nb uniquely suited for applications where superconductivity is required in the presence of (relatively) large magnetic fields. One such example is its use in superconducting radio frequency (SRF) cavities,<sup>2,3</sup> which make up many accelerator beamlines (for charged particles) across the globe. In the pursuit of optimal accelerating efficiency and cryogenic operation economy, there is great interest in *engineering* Nb to remain in the Meissner state up to the highest magnetic fields possible. This can be achieved empirically by chemically modifying its surface through baking<sup>4,5</sup> or doping,<sup>6,7</sup> as well as by coating it with thin layers of other superconducting (and insulating) materials.<sup>8–13</sup>

To better understand how these microscopic modifications affect Nb's superconducting properties, an experimental technique capable of interrogating the *local* electromagnetic fields in the near surface region is essential. Similarly, as the material properties are expected to vary below the surface, *spatial* resolution is also a requirement. In reality, there are few experimental techniques capable of simultaneously satisfying these criteria. Perhaps the most widely known is low-energy muon spin rotation (LE- $\mu$ SR),<sup>14,15</sup> which uses implanted positive muons  $\mu^+$  as local magnetic probes of the field inside. Indeed, LE- $\mu$ SR has been used to study Meissner screening in Nb, revealing: the importance of non-local electrodynamics<sup>16,17</sup> and strong-coupling corrections<sup>18</sup> in “clean” samples;<sup>19</sup> the dependence of the magnetic penetration depth on film preparation technique;<sup>20</sup> as well as an “anomalous” modification to the screening profile for select surface treatments.<sup>21</sup> As the latter result is controversial,<sup>22,23</sup> it is imperative that alternative means of study be developed to corroborate such findings. To this end, here we employed a lesser-known (but closely related) technique — ion-implanted  $\beta$ -detected nuclear magnetic resonance ( $\beta$ -NMR) — to study the superconducting properties of Nb below its surface. Thorough accounts of the  $\beta$ -NMR technique can be found in several recent<sup>24,25</sup> and older<sup>26,27</sup> review articles, with additional details given in several technical overviews.<sup>28–30</sup>

In ion-implanted  $\beta$ -NMR,<sup>24,25</sup> a radioactive spin probe is “inserted” into a material of interest and its nuclear magnetic resonance (NMR) response is monitored through the anisotropic property of  $\beta$ -decay (see e.g.,<sup>31</sup>), analogous to the

<sup>a</sup>E-mail: [rmlm@triumf.ca](mailto:rmlm@triumf.ca)

<sup>b</sup>Current address: JSI Telecom, 99 Michael Cowpland Dr, Kanata, ON K2M 1X3, Canada

<sup>c</sup>Current address: Australia's Nuclear Science and Technology Organisation, New Illawarra Road, Lucas Heights, NSW 2234, Australia

<sup>d</sup>Current address: D-Wave Systems Inc., 3033 Beta Avenue, Burnaby, BC V5G 4M9, Canada

<sup>e</sup>Current address: Angstrom Vision Inc., 2-831 3rd St W, North Vancouver, BC V7P 3K7, Canada

<sup>f</sup>E-mail: [junginger@uvic.ca](mailto:junginger@uvic.ca)

detection scheme used in LE- $\mu$ SR.<sup>14,15,32</sup> Just as in “conventional” NMR using stable nuclei (see e.g.,<sup>33–36</sup>),  $\beta$ -NMR is sensitive to the electronic and magnetic properties of the “host” material; however, its sensitivity (per nucleus) is greater by a factor of  $\sim 10^{10}$ , allowing for the study of situations typically inaccessible by NMR (e.g., thin films,<sup>37–40</sup> heterostructures,<sup>41–44</sup> or isolated impurities<sup>45,46</sup>). Supplementing this feature is the ability to control the implantation energy that the probe radioisotope is ion-implanted, allowing for it to be “placed” at specific depth ranges. This further extends the types of problems that can be studied, especially those where *depth-resolution* is essential. For example, the depth-resolution afforded by  $^8\text{Li}$   $\beta$ -NMR has been used to investigate: molecular dynamics in glassy polystyrene,<sup>47–49</sup> the magnetism of  $\text{Mn}_{12}$  single-molecule magnets;<sup>50</sup> surface magnons in antiferromagnetic  $\text{Fe}_2\text{O}_3$ ;<sup>51</sup> finite size effects in Pd thin films;<sup>39</sup> as well as the superconductor  $\text{NbSe}_2$  in both the vortex<sup>52</sup> and Meissner<sup>53</sup> states.

While LE- $\mu$ SR and  $\beta$ -NMR are largely complementary techniques,<sup>54</sup> differences in probe properties (e.g., radioactive lifetime) make  $\beta$ -NMR much more amenable to the measurement of phenomena transpiring over longer timescales, such as spin-lattice relaxation (SLR) (in non-magnetic materials). SLR is driven by stochastic fluctuations in the local electromagnetic field at the probe’s stopping site, which dynamically “re-orient” the probe’s spin, returning the polarization of the ensemble to  $\sim 0$  (i.e., its thermal equilibrium value). When the “host” contains an abundance of isotopes with non-zero nuclear spin, the implanted probe couples to the “bath” of host spins via the dipolar interaction, providing a relaxation “channel” with sensitivity to the static component of the local field. This form of “cross-relaxation” (see e.g.,<sup>55</sup>) has been used to study the magnetic penetration depth in the multi-band superconductor  $\text{NbSe}_2$ ,<sup>53</sup> as well as order-parameter fluctuations in superconducting Pb and Ag/Nb thin films,<sup>56</sup> by way of the  $\beta$ -NMR probe  $^8\text{Li}$ . Here, we applied and extended this methodology to extract the Meissner screening profile in a Nb(300 nm)/ $\text{Al}_2\text{O}_3$  thin film. Specifically, in a 20 mT applied magnetic field, we measured the temperature and implantation energy (i.e., depth) dependence of implanted  $^8\text{Li}$ ’s SLR rate  $1/T_1$ , revealing a sharp increase in relaxation at temperatures below  $T_c$ , whose magnitude increases deeper below the material’s surface. By contrast, this depth-dependence vanishes in the normal state, consistent with the expected signature for Meissner screening.<sup>53,56</sup> From a fit of the data to a model accounting for  $1/T_1$ ’s dependence on temperature, implantation energy, and magnetic field, we determined that the screening profile is well-described by a simple London model<sup>57,58</sup> with a magnetic penetration depth exceeding Nb’s “intrinsic” value. The result is consistent with similarly prepared films, known to possess relatively short carrier mean-free-paths.

The rest of the manuscript is organized as follows. Details of the  $\beta$ -NMR experiments are given in Section II, along with information on the preparation of our Nb sample (Section II B). Our results and analysis are presented in Section III, with a description of our data given in Section III A, followed by an account of our analysis approach (Section III B), and the modelling of the extracted results (Section III C). We discuss our

findings and their implications in Section IV, and a summary is given in Section V.

## II. EXPERIMENT

$\beta$ -NMR experiments were performed at TRIUMF’s isotope separator and accelerator (ISAC) facility in Vancouver, BC, Canada. The probe radioisotope  $^8\text{Li}$  (nuclear spin  $I = 2$ ; gyromagnetic ratio  $\gamma/(2\pi) = 6.302\,21(7)$  MHz  $\text{T}^{-1}$ ,<sup>59,60</sup> electric quadrupole moment  $Q = +31.4(2)$  mb;<sup>61</sup> radioactive lifetime  $\tau_\beta = 1.2096(5)$  s;<sup>62</sup> and mass  $m_{^8\text{Li}} = 8.022\,486\,24(5)$  u<sup>63,64</sup>) was generated from an isotope production target (e.g., Ta foil stacks)<sup>65</sup> irradiated with a  $\sim 500$  MeV proton beam at a current on the order of  $\sim 20$   $\mu\text{A}$ . The target, heated in excess of  $\sim 2000$  K to accelerate thermal out-diffusion of  $^8\text{Li}$ , was coupled to a surface ion source<sup>65</sup> and a mono-energetic  $\sim 20$  keV beam of  $^8\text{Li}^+$  was extracted with an intensity of  $\sim 10^7$  ions/s. A high-resolution magnetic dipole mass separator was used to ensure the isotopic purity of the beam, which was transported through a high vacuum beamline via electrostatic optics. During transport, the ion beam was neutralized in-flight and subsequently spin-polarized by collinear optical pumping with circularly polarized resonant laser light,<sup>28</sup> yielding a high degree of nuclear spin-polarization ( $\sim 70\%$ <sup>66,67</sup>). The highly polarized beam was then re-ionized and (electrostatically) steered to the spectrometer,<sup>24,29</sup> where the probe  $^8\text{Li}^+$  ions were implanted into the Nb thin film, which was affixed to a holder compatible with the spectrometer’s cold-finger cryostat. The energy of the ion beam was controlled by biasing the spectrometer’s platform to high positive voltage (up to 20 kV), electrostatically decelerating the  $^8\text{Li}^+$  from their transport energy (within the final few centimeters of their trajectory) before implantation. Note that, in the lead-up to implantation, the  $^8\text{Li}$  spin-polarization is parallel to the film’s surface and the applied field, but perpendicular to the beam’s momentum (see e.g.,<sup>29</sup>).

An essential aspect of this approach is the spatial (i.e., depth) resolution obtained through ion-implanting our  $\beta$ -NMR probe  $^8\text{Li}$  into Nb. Ion-implantation is a controlled, non-equilibrium means of introducing impurities in solids, which finds use (on an industrial scale), for example, in the electrical doping of semiconductors (see e.g.,<sup>72</sup>). During implantation, the “injected” ion loses energy through its interaction with the host’s electrons and nuclei, amounting to a series of (dampened) collisions that thermalize the projectile. The slowing process is stochastic, resulting in a *distribution* of stopping positions for a mono-energetic projectile. This process can be simulated accurately using Monte Carlo methods (see e.g.,<sup>68,73</sup>), and the results from such simulations are used to connect the probe’s NMR response with a spatial region of the sample, just as in LE- $\mu$ SR.<sup>74,75</sup> Several implantation profiles for 2 keV to 20 keV  $^8\text{Li}^+$  stopping in Nb, simulated using the SRIM Monte Carlo code,<sup>68,69</sup> are shown in Figure 1.

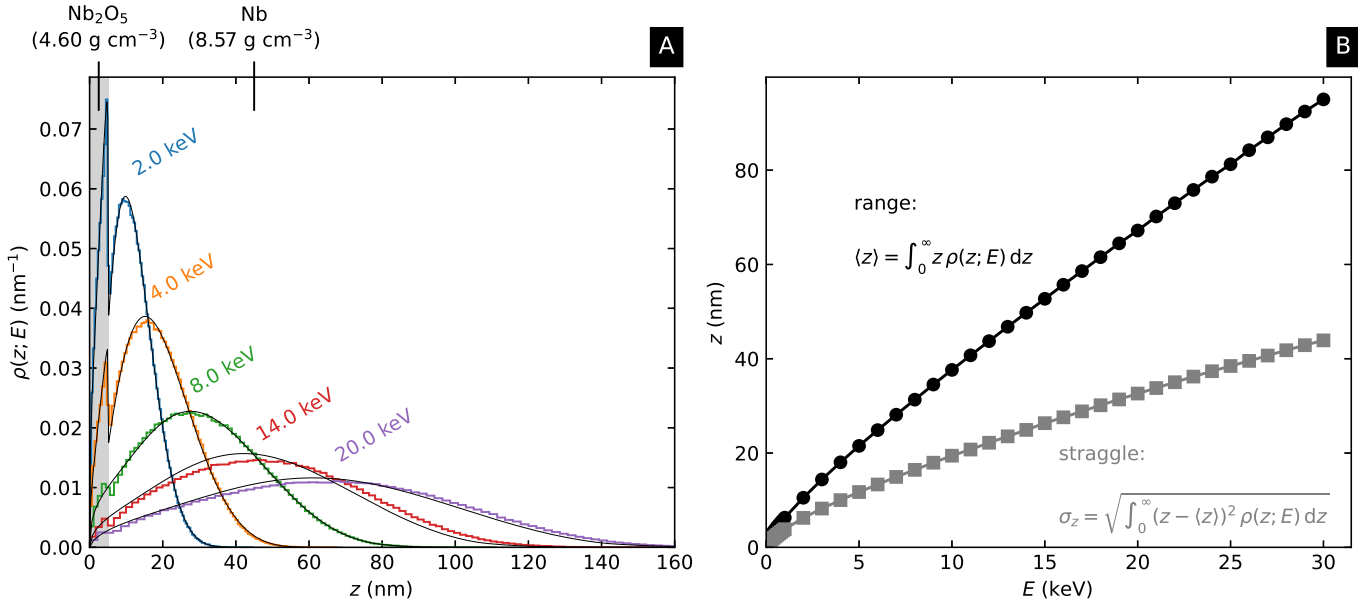


FIG. 1. Results from simulations of  $10^6$   ${}^8\text{Li}^+$  ions implanted in a  $\text{Nb}_2\text{O}_5(5\text{ nm})/\text{Nb}$  target, calculated using the SRIM Monte Carlo code<sup>68,69</sup> by aid of the Python package pysrim.<sup>70</sup> (A): Typical  ${}^8\text{Li}^+$  stopping profiles at select implantation energies  $E$  are shown, represented here as histograms (with 100 bins) of the stopping probability  $\rho(z; E)$  vs. depth below the surface  $z$ . The thin black lines denote fits to a phenomenological model for  $\rho(z; E)$  [Equations (15) and (16) — see Section III C], capturing all features of the stopping profiles at each energy. Note that the abrupt change in  $\rho(z; E)$  at the  $\text{Nb}_2\text{O}_5/\text{Nb}$  boundary is related to the different layer densities (indicated in the inset). The thickness of the surface pentoxide oxide layer (5 nm) is typical for Nb (see e.g.,<sup>71</sup>). (B): Moments of the stopping profiles. As  $E$  increases, so does the  ${}^8\text{Li}^+$  range and straggle (i.e., the mean,  $\langle z \rangle$ , and standard deviation,  $\sigma_z$ ).

## A. Measurements

In each  $\beta$ -NMR measurement, the  ${}^8\text{Li}$  spin-polarization was monitored after implantation through the anisotropy of its radioactive  $\beta$ -decay.<sup>31</sup> Specifically, the experimental asymmetry  $A$  (proportional to the average longitudinal spin-polarization  $p_z$ ) was measured by combining the  $\beta$ -rates in two opposed scintillation counters.<sup>24</sup> In our measurements, the sense of circular polarization (left and right) of the pumping laser light was also alternated,<sup>28</sup> producing either “positive” or “negative” helicity in the  ${}^8\text{Li}^+$  beam (i.e., its nuclear-spin polarization is aligned or counter-aligned with the beam direction). Data were collected separately for each helicity and then combined to remove detection systematics (see e.g.,<sup>24,27</sup>). Explicitly, the well-known “four-counter” method was used:

$$A = \frac{1-r}{1+r} \equiv A_0 p_z, \quad (1)$$

where

$$r \equiv \sqrt{\frac{(L_+/R_+)}{(L_-/R_-)}}$$

is the geometric mean of the ratio of rates in the opposing counters  $L$  and  $R$  for the  $\pm$  polarization senses. Note that the proportionality constant between  $A$  and  $p_z$ , denoted as  $A_0$  in Equation (1), depends on both the experimental geometry and the details of the  $\beta$ -decay (on the order of  $\sim 10\%$  here).

SLR measurements were performed by monitoring the transient decay of spin-polarization both during and following a short pulse of beam of duration  $\Delta$  (typically  $\sim 4$  s). During the pulse, the polarization approaches a steady-state value, while after the pulse, it relaxes to essentially zero. At the edge of the pulse, there is a discontinuity in the slope, characteristic of  $\beta$ -NMR SLR data acquired in this manner.<sup>24,25</sup> This bipartite behavior can be described quantitatively by considering a uniform distribution of probe arrival times (i.e., a time-independent  ${}^8\text{Li}^+$  production rate). Explicitly, for an arrival time  $t'$ , the temporal evolution of nuclear spin-polarization at time  $t > t'$  follows:

$$p_z(t) = p_0 \times \begin{cases} \frac{\int_0^t \exp[-(t-t')/\tau_\beta] R(t,t') dt'}{\int_0^t \exp[-t'/\tau_\beta] dt'}, & t \leq \Delta, \\ \frac{\int_0^\Delta \exp[-(t-t')/\tau_\beta] R(t,t') dt'}{\exp[-(t-\Delta)/\tau_\beta] \int_0^\Delta \exp[-t'/\tau_\beta] dt'}, & t > \Delta, \end{cases} \quad (2)$$

where  $p_0 \approx 70\%$  is the degree of nuclear spin-polarization produced from optical pumping,<sup>66,67</sup> and  $R(t,t')$  is a “relaxation” function describing the decay of  $p_z$  (e.g., an exponential in the simplest case). Note that, unlike in conventional NMR, no transverse radio frequency (RF) field  $B_1$  is required for measurement of the SLR, meaning that there is no intrinsic spectral resolution of the relaxation, which represents the SLR of the *entire*  $^8\text{Li}$  population (i.e., not just those with observable resonances). A typical SLR measurement required  $\sim 30$  min, corresponding to  $\sim 10^8$  total decay events.

## B. Sample

A 300 nm Nb thin film from a previous  $\beta$ -NMR experiment<sup>76</sup> was employed in this study. The film was grown ( $1 \text{ \AA s}^{-1}$  deposition rate) by RF sputtering a 99.9% Nb target (Goodfellow) onto an  $8 \text{ mm} \times 12 \text{ mm} \times 0.5 \text{ mm}$  epitaxially polished  $\text{Al}_2\text{O}_3$   $\langle 0001 \rangle$  substrate (Honeywell) at  $\sim 50^\circ\text{C}$  in 3 mTorr of Ar ( $25 \text{ cm}^3 \text{ min}^{-1}$  flow), resulting in a high degree of orientation in the  $\langle 110 \rangle$  direction (confirmed by x-ray diffraction (XRD)). The film had a bulk critical temperature  $T_c \approx 8.9 \text{ K}$ , as determined from magnetometry measurements. Further characterization details are given elsewhere.<sup>76</sup>

## III. RESULTS & ANALYSIS

This section is divided into three parts. First, we present the raw SLR data and describe its features in Section III A. Subsequently, we consider the analysis of the SLR data and show the extracted SLR rates ( $1/T_1$ ) in Section III B. Finally, in Section III C, we construct a model for  $1/T_1$  that allows for the extraction of the magnetic penetration depth and apply it to the results.

### A. SLR Data

Typical  $^8\text{Li}$  SLR data in Nb at low temperatures and magnetic fields are shown in Figure 2. In all cases, the SLR is orders of magnitude faster than in fields on the order of  $\sim 1 \text{ T}$ ,<sup>76</sup> typical of measurements in the field regime where low-frequency fluctuations of the “host” *nuclear* spins provide the dominant relaxation mechanism (see e.g.,<sup>53,77</sup>). The relaxation, however, while fast relative to the “natural” timescale

of the probe ( $\sim 1/\tau_\beta$ ), remains observable for all conditions investigated here. From the temperature dependent measurements at a constant implantation energy  $E = 19.9 \text{ keV}$  (i.e.,  $\langle z \rangle \approx 70 \text{ nm}$ ), it is apparent that, upon cooling the sample from the normal state ( $T > T_c$ ) to the Meissner state ( $T < T_c$ ), the SLR rate increases (as evidenced by the increased haste in the decay of the SLR “curves”). This SLR behavior is consistent with that observed in other superconductors.<sup>53,56</sup> Similarly, from measurements at constant temperature  $T = 3.5 \text{ K}$  (well into the Meissner state), it is clear that as the implantation energy increases (equivalent to  $^8\text{Li}$  sampling deeper below Nb’s surface), so too does the SLR rate. Note that equivalent measurements in the normal state ( $T > T_c$ ) show no such dependence on  $E$ , suggesting that this SLR response is a result of Nb’s superconductivity. Interestingly, we note that the data in Figure 2 includes measurements both where the applied field is zero during cool-down (zero-field-cooled) and when it is 20 mT (field-cooled), showing no appreciable differences (see below).

### B. Quantifying $1/T_1$

To quantify the observations outlined in Section III A, we consider a model to determine the SLR rate  $1/T_1$ . First, we remark that, in contrast to measurements at higher fields,<sup>76</sup> the decay of the SLR “curves” is *non-exponential* at all measured conditions. This isn’t unprecedented for a spin  $I = 2$  nucleus, though it is difficult to identify the exact underlying cause (e.g.,<sup>78–81</sup>), which may be complicated by a fundamental change in the character of the SLR at low magnetic fields (see e.g.,<sup>77</sup>). This detail is compounded by the fact that there are *two*  $^8\text{Li}^+$  stopping sites in Nb at low temperature.<sup>76</sup> While an atomistic model of the stopping sites may illuminate the matter, it is still forthcoming.<sup>82</sup> Consequently, we elected for a pragmatic approach and fit the SLR data using a (phenomenological) stretched exponential “relaxation” function. For a uniform distribution of probe arrival times (i.e., a time-independent  $^8\text{Li}^+$  production rate),  $R(t,t')$  from Equation (2) takes the form:

$$R(t,t') = \exp\left[-\left(\frac{t-t'}{T_1}\right)^\beta\right], \quad (3)$$

where  $1/T_1$  is the SLR rate, and  $\beta \in (0, 1]$  is the stretching exponent. While a value of  $\beta < 1$  modifies the form of an exponential decay, equivalent to the presence of faster (slower)

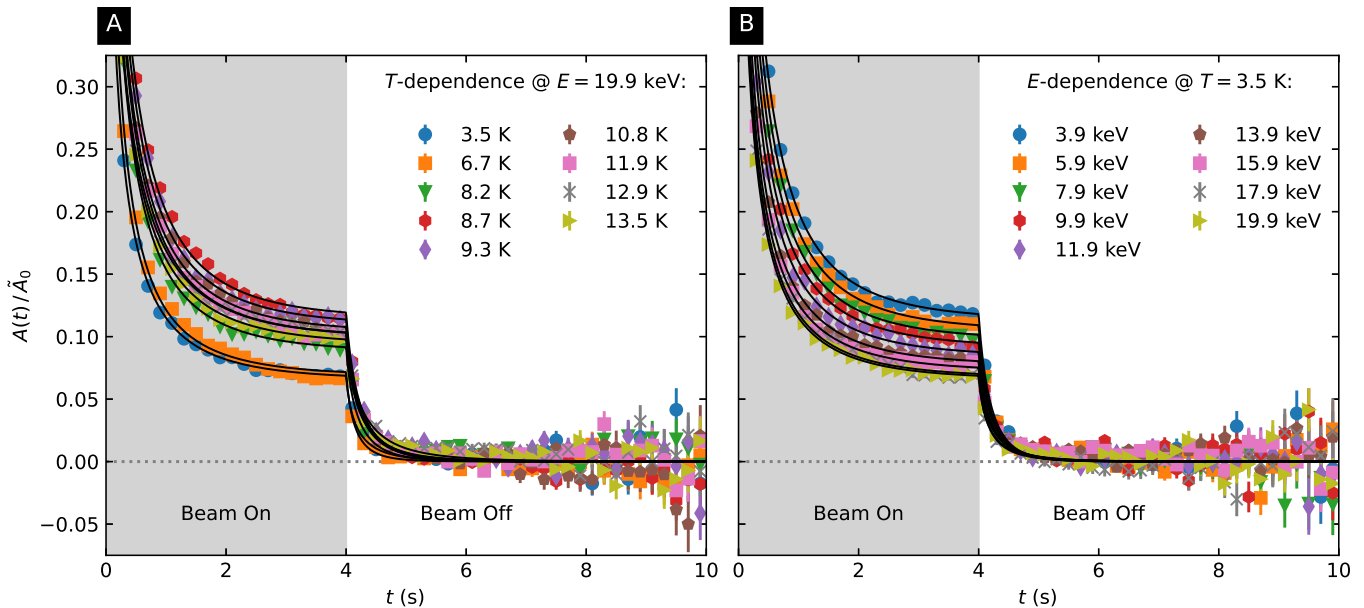


FIG. 2. Typical  ${}^8\text{Li}$  SLR data in Nb(300 nm)/ $\text{Al}_2\text{O}_3$  at low temperatures  $T < 15$  K and implantation energies  $E \leq 20$  keV (where all implanted  ${}^8\text{Li}^+$  stops in the film — see Figure 1) in an applied magnetic field  $B_0 = 20$  mT parallel to the sample surface. The data (represented as histograms) have been binned by a factor of 20 for clarity and the solid lines represent fits using a stretched exponential relaxation function (described in Section III B). In all cases, the SLR rate is orders of magnitude faster than at higher fields<sup>76</sup> with much of the (normalized) asymmetry  $A(t)/\tilde{A}_0$  vanishing within the first few milliseconds (the vertical scale has been adjusted to better show the remaining signal). (A): Temperature dependent measurements at a constant implantation energy  $E = 19.9$  keV. Upon cooling the sample from the normal state ( $T > T_c$ ) to the Meissner state ( $T < T_c$ ) the SLR rate increases, as evidenced by the increased haste in the decay of the “curves”. (B): Implantation energy dependent measurements at a constant temperature  $T = 3.5$  K. In the Meissner state, as the implantation energy increases (equivalent to  ${}^8\text{Li}$  sampling deeper below Nb’s surface) the SLR rate increases. Note that equivalent measurements in the normal state ( $T > T_c$ ) show no such dependence on energy.

relaxation at early (late) times, the quantity  $T_1$  captures the characteristic  $1/e$  decay time of  $p_z$ . We note that this model accurately describes the data over *all* measurement conditions, without over-parameterization<sup>83</sup>.

The SLR data were fit using Equations (1) to (3). Note that, for this definition of  $A(t)$ , the terms  $A_0$  and  $p_0$  are not uniquely defined and instead we used a single “effective” parameter,  $\tilde{A}_0 \equiv A_0 p_0$ , which is on the order of  $\sim 10\%$  for our data. Similarly, to mitigate the known “inflation” of  $\tilde{A}_0$  from Equation (3) (i.e., from the divergence in Equations (2) and (3) when  $t \rightarrow 0$  s), we constrained our fits such that  $\tilde{A}_0$  was shared across measurements at constant  $E$  (i.e., in a so-called “global” fit). Empirically,  $\tilde{A}_0$  was found to vary with  $E$  according to a piecewise linear function (i.e., with different slopes above and below  $\sim 4$  keV) and we imposed the additional constraint that it must fall along this line<sup>84</sup>. Lastly, we point out that for our  $R(t, t')$ , numeric integration is required to evaluate Equation (2). For this, we used tanh-sinh quadrature,<sup>85,86</sup> (i.e., a so-called “double-exponential” technique), which provides both accurate and expedient evaluation of our model. The fit quality was good for all the SLR data, with a typical reduced  $\chi^2 \approx 1.02$  for each measurement. The fitting was performed by a custom Python script using the mudpy, bdata, and bfit libraries.<sup>87,88</sup> A subset of the fit results are shown in Figure 2, with the SLR rates and stretching exponents extracted from the analysis presented in Figures 3 and 4.

We now consider the results from fitting. In the normal state below  $\sim 15$  K,  $1/T_1$  varies approximately linearly with temperature (see Figure 3); however, its slope is much larger than in measurements at higher field,<sup>76</sup> resembling the  ${}^8\text{Li}$  SLR in Au<sup>77</sup> and other elemental metals.<sup>93</sup> Similarly, the (extrapolated) intercept of  $1/T_1$  at 0 K is also non-zero. Note that these two features are inconsistent with the so-called Korringa response<sup>35,89</sup> expected for relaxation due to electrons in a metal’s conduction band. We shall return to this point below.

Just below the film’s “bulk”  $T_c \approx 8.9$  K, there is a pronounced “kink” in the temperature dependence of  $1/T_1$ . The discontinuity at  $\sim 8.8$  K is suggestive of a transition temperature, with the shift to lower- $T$  being consistent with the suppression of  $T_c$  by the small (20 mT) applied field. As the temperature is lowered further,  $1/T_1$  increases non-linearly, with the sharpest increase occurring within the first few Kelvin below the “kink”. At colder temperatures, the increased SLR ceases, with  $1/T_1$  saturating by  $\sim 4$  K. This  $1/T_1$  “dome” is consistent with the expected  ${}^8\text{Li}$  SLR signature for Meissner screening.<sup>53,56</sup> Interestingly, as noted earlier, both field- and zero-field-cooled measurements are in good agreement with each other, suggesting that either flux trapping has little influence on the observed SLR rates or there is little flux trapped in the film.

Interestingly, we find a stretching exponent  $\beta$  close to  $\sim 0.5$  at all measurement conditions, showing only weak variation with

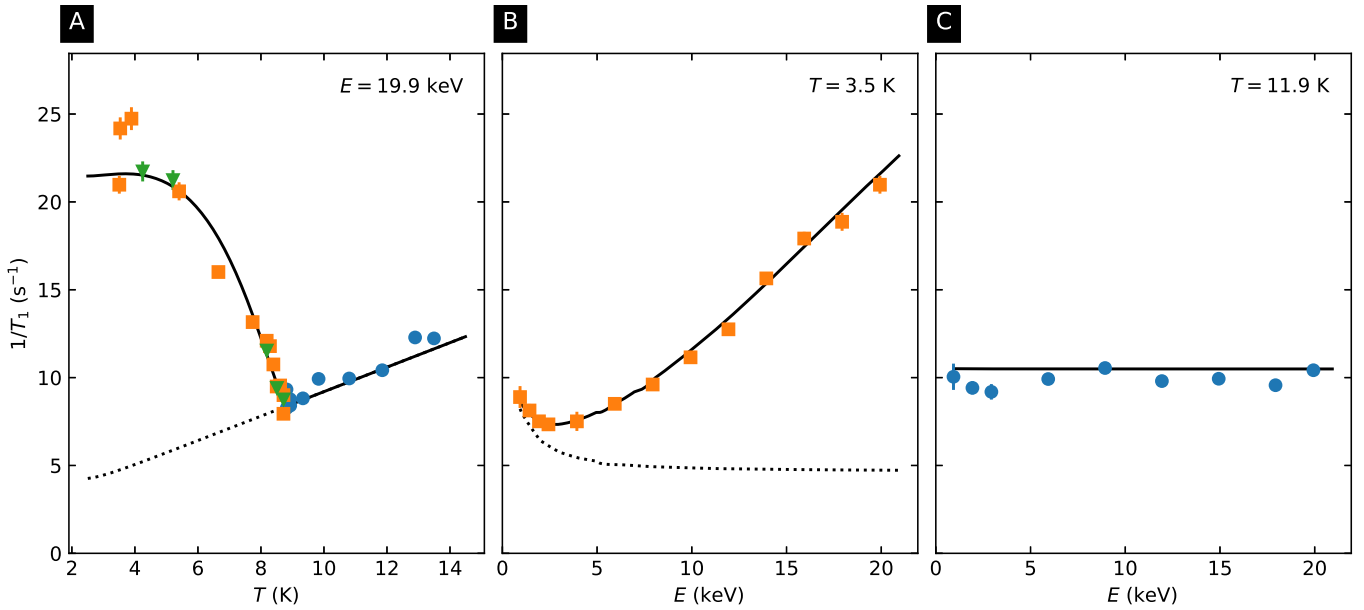


FIG. 3.  $^8\text{Li}$  SLR rates  $1/T_1$  in Nb(300 nm)/Al<sub>2</sub>O<sub>3</sub> at 20 mT parallel to its surface, determined from fits to a stretched exponential model [Equations (1) to (3)] described in the text. The symbols distinguish different groups of data [normal state (●); Meissner state, field-cooled (■); Meissner state, zero-field-cooled (▼)], all in good agreement with each other. The solid black line (—) denotes a fit of the  $1/T_1(E, T, B)$  model to *all* the data, clearly capturing all of the main features. For comparison, the dotted black line (· · ·) shows the predicted normal-state response for the SLR rate. (A) Temperature dependence of  $1/T_1$  at constant implantation energy ( $E = 19.9$  keV), corresponding to a mean stopping depth of  $\sim 90$  nm. In the normal state, the SLR rate varies linearly with temperature, but is orders of magnitude larger than the electronic (i.e., Korringa<sup>35,89</sup>) relaxation observed at higher applied fields.<sup>76</sup> At  $T_c \approx 8.8$  K, there is a pronounced kink in the temperature dependence and  $1/T_1$  increases substantially with decreasing  $T$ . This is the manifestation of Meissner screening sensed through the dipole-dipole coupling (i.e., “cross-relaxation”) with the Nb host’s nuclear spins (see e.g.,<sup>53,56</sup>). (B) Implantation energy dependence of  $1/T_1$  at constant temperature in the Meissner state ( $T = 3.5$  K). At energies  $>4$  keV, the SLR rate increases monotonically with increasing  $E$ , consistent with enhanced field screening deeper below the surface. At energies  $\leq 4$  keV, there is a small upturn in  $1/T_1$  with decreasing  $E$ , likely a result of a (weak) paramagnetic contribution from the native oxide layer at the Nb surface.<sup>90,91</sup> (C) Implantation energy dependence of  $1/T_1$  at constant temperature in the normal state ( $T = 11.9$  K). In contrast to the data in the Meissner state, no meaningful energy (i.e., depth) dependence is observed.

TABLE I. Summary of the main fit parameters and their uncertainties (rounded according to the Particle Data Group’s rules<sup>92</sup>), determined from fits of the  $1/T_1(E, B, T)$  model to the data in Figure 3 (solid black line). For convenience, a brief description of each parameter and a list of equations where they appear are also included. Further details about the model and fitting procedure are given in Section III C.

Symbol	Value	Units	Description	Appearances
$d$	$5.0 \pm 0.9$	nm	thickness of the non-superconducting “dead layer” at the film’s surface	Equation (12)
$\lambda$	$51.5 \pm 2.2$	nm	the film’s magnetic penetration depth	Equations (12) and (13)
$B_d$	$(41.1 \pm 2.1) \times 10^{-6}$	T	magnitude of the dipolar field at the $^8\text{Li}$ stopping sites	Equation (8)
$\tau_c$	$(6.1 \pm 0.5) \times 10^{-6}$	s	NMR correlation time for the fluctuations causing SLR	Equation (9)
$T_c$	$8.775 \pm 0.014$	K	the film’s superconducting transition temperature	Equation (13)
$c$	$0.697 \pm 0.011$	$\text{s}^{-1} \text{K}^{-1}$	slope of the $T$ -linear contribution to the total SLR rate	Equation (7)
$C$	$(2.03 \pm 0.19) \times 10^3$	$\text{s}^{-1} \text{K}^b$	constant in the near-surface paramagnetic SLR contribution	Equation (14)
$b$	4.5		exponent in the near-surface surface paramagnetic SLR contribution	Equation (14)

temperature or implantation energy (see Figure 4). Above Nb’s  $T_c$ ,  $\beta$  is nearly constant and independent of  $E$ , showing only a small degree of scatter. Near  $T_c$ , a small local maximum is observed, with the exponent decreasing smoothly as the temperature is lowered. At the lowest measured temperature ( $\sim 3.5$  K), some  $E$ -dependence to  $\beta$  is evident, with  $\beta$  increasing with decreasing  $E$ , implying the SLR becomes more homogeneous closer to the sample’s surface. While  $\beta = 0.5$

is often ascribed to heterogenous relaxation resulting from, for example, spatial disorder,<sup>78</sup> its absence at high field<sup>76</sup> suggests it must be of a different origin (cf. the field-dependent  $^8\text{Li}$  SLR in Au<sup>77</sup>). Given the ambiguity of isolating the cause the non-exponential SLR transients, we suggest that the  $\beta$  of  $\sim 0.5$  represents an effective average over all relaxing  $^8\text{Li}$ , whose SLR time-constants are too similar to isolate here.

Lastly, we note that the implantation energy dependence in

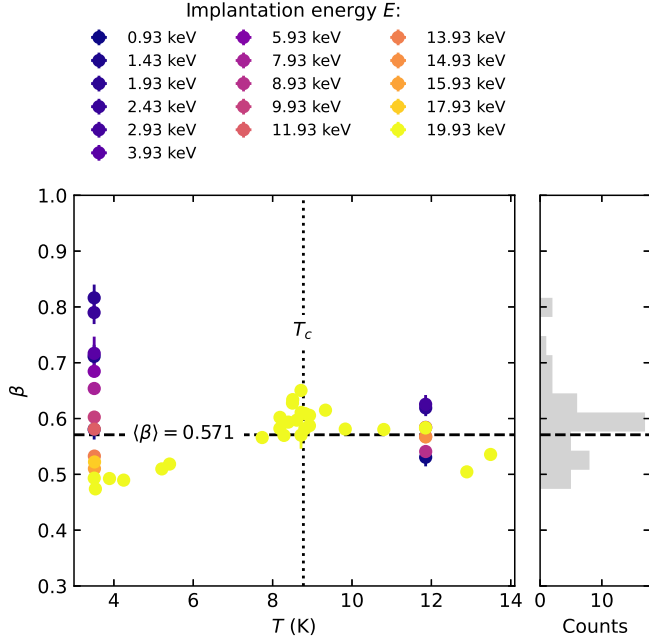


FIG. 4. The temperature ( $T$ ) and implantation energy ( $E$ ) dependence of the stretching exponent  $\beta$ , determined from fits of the  $^8\text{Li}$  SLR data (Figure 2) to a stretched exponential relaxation function [Equation (3)].  $\beta$  is found to be weakly dependent on both  $T$  and  $E$ , but remains close to  $\sim 0.5$  for the majority of our measurement conditions. Above Nb's critical temperature  $T_c$  (indicated by the vertical dotted line),  $\beta$  is nearly constant and independent of implantation energy  $E$ , showing only a small degree of scatter. At  $T_c$ , a small local maximum is observed, with the exponent decreasing smoothly as the temperature is lowered. At  $\sim 3.5$  K (i.e., well into the Meissner state), the  $E$ -dependence is most pronounced, with the (depth-averaged) relaxation becoming increasingly homogeneous with decreasing  $E$ . The exponent's average value ( $\langle\beta\rangle \approx 0.571$ ) is indicated by the horizontal dashed line, with the value included in the inset. The distribution of  $\beta$  values is also shown as a histogram.

the Meissner state (3.5 K) appears more complicated than anticipated. As  $E$  increases,  $1/T_1$  decreases slightly, reaching a minimum around  $\sim 2.5$  keV (i.e.,  $\langle z \rangle \approx 10$  nm); however, for all higher  $E$ ,  $1/T_1$  increases monotonically, qualitatively consistent with the expected SLR response from Meissner screening.<sup>53,56</sup> This rich behavior in the Meissner state is greatly contrasted by that in the normal state above  $T_c$ , where any (meaningful) depth-dependence to  $1/T_1$  is absent. This fact is strong confirmation that the observed effects originate from Nb's superconductivity.

With the essential features of the  $1/T_1$  data described above, we now consider a model that captures these details, including the magnetic penetration depth  $\lambda$ .

### C. The $1/T_1$ Model

First, we remark that for a given  $^8\text{Li}^+$  implantation energy  $E$ , the measured  $1/T_1$  represents an average over the probe's

stopping profile  $\rho(z; E)$ :

$$\frac{1}{T_1} \equiv \int_0^\infty \frac{1}{T_1(z)} \rho(z; E) dz, \quad (4)$$

where the term  $1/T_1(z)$  encapsulates any depth dependence of the SLR rate<sup>94</sup>. While  $\rho(z; E)$  can be reliably determined from Monte Carlo simulations (see Section II and fig. 1), we must postulate a realistic form for  $1/T_1(z)$ . In general, there can be several contributions to the *observed* SLR rate  $1/T_1$ , which can be decomposed into distinct mechanisms<sup>95</sup>:

$$\frac{1}{T_1} = \frac{1}{T_1^e} + \frac{1}{T_1^d} + \frac{1}{T_1^q} + \dots$$

Here, the  $1/T_1^i$ s denote contributions from: conduction electrons ( $i = e$ ), dipole-dipole interactions ( $i = d$ ), and quadrupolar interactions ( $i = q$ ). While other contributions are possible,<sup>33–36</sup> we restrict ourselves to the most common ones listed above.

We begin by considering  $1/T_1^e$ . In metals, the SLR is often dominated by the so-called Korringa mechanism,<sup>35,89</sup> wherein relaxation is induced by spin-flip scattering of conduction electrons coupled to the nuclear spin via their hyperfine interaction. From a derivation based on Fermi's golden rule, the sum over electron momenta, when converted to an integral over energy, yields:

$$\frac{1}{T_1^e} = \frac{2\pi}{\hbar} A_{\text{hf}}^2 \int_{-\infty}^{+\infty} \rho_e^2(E) f(E) [1 - f(E)] dE, \quad (5)$$

where  $A_{\text{hf}}$  is the hyperfine coupling,  $\rho_e(E)$  is the electronic density of states (DOS), and  $f(E)$  is the Fermi-Dirac distribution:

$$f(E) = \left[ \exp\left(\frac{E - E_F}{k_B T}\right) + 1 \right]^{-1},$$

with  $E_F$  and  $k_B$  denoting the Fermi energy and Boltzmann constant, respectively. Note that the above integral is over all electron energies in the conduction band. In a broad band degenerate metal, where  $E_F \gg k_B T$ ,  $\rho_e(E)$  is practically constant over the range where the Fermi factor  $f(E)[1 - f(E)]$  is non-zero, and the integral (to an excellent approximation) evaluates to:

$$\frac{1}{T_1^e} \approx \frac{2\pi}{\hbar} A_{\text{hf}}^2 \rho_e^2(E_F) k_B T. \quad (6)$$

The salient feature of Equation (6) is its linear temperature dependence, which is distinct from most other SLR mechanisms. This also produces an SLR rate that is *independent* of the applied magnetic field. This electronic relaxation has been reported previously for  $^8\text{Li}$  implanted in this Nb film,<sup>76</sup> where below  $\sim 20$  K:

$$\frac{1}{T_1^e T} \approx 1.271(39) \times 10^{-2} \text{ s}^{-1} \text{ K}^{-1}.$$

Importantly, these rates are at least an order of magnitude smaller than our observed  $1/T_1$ s, leading us to conclude that

the importance of  $1/T_1^e$  is negligible at our measurement conditions<sup>96</sup>.

Next we consider  $1/T_1^q$ . The  $^8\text{Li}$  resonance in Nb at low temperatures shows unambiguously that some of the probes stop in sites with non-cubic symmetry,<sup>76</sup> where a static (i.e., time-averaged) electric field gradient (EFG) remains finite. Considering Nb's body-centred cubic (BCC) structure,<sup>97</sup> there is some difficulty in precisely assigning a stopping site. Earlier work suggested the possibility of an interstitial dumbbell-like  $^8\text{Li}$ –Nb defect complex at low- $T$ ,<sup>76</sup> which is consistent with preliminary results from density functional theory (DFT) calculations;<sup>82</sup> however, no firm assignment has yet been made. We note though that the presence of a non-zero *static* EFG does not necessitate a dynamic component sufficient for causing SLR (cf.  $^8\text{Li}$   $\beta$ -NMR in Bi<sup>98</sup>). Moreover,  $1/T_1^q$  is expected to follow a power-law that is strongly dependent on temperature,<sup>99</sup> but not applied field, which is inconsistent with our data and measurements at higher fields.<sup>76</sup> At our measurement conditions, such a phonon-mediated mechanism should be negligible, given that  $T$  is far below Nb's Debye temperature ( $\sim 270$  K) and there are very few thermally populated phonons. On that basis, we rule it out as a significant source for our  $1/T_1$ <sup>100</sup>.

With the above two mechanisms ruled out as meaningful contributors, it is curious that a  $T$ -linear component of the SLR rate persists; however, this is not a novel observation and similar behavior has been observed in the  $^8\text{Li}$   $\beta$ -NMR of materials whose NMR response is metallic (see e.g.,<sup>77,101,102</sup>). As the exact origin remains unclear, we adopted an empirical term in our model:

$$\frac{1}{T_1^l} \approx c \times T, \quad (7)$$

where  $\langle \delta B_d^2 \rangle$  is the mean-squared fluctuating field<sup>109</sup> and

$$J_n(\omega_i) = \frac{\tau_c}{1 + \omega_i^2 \tau_c^2}, \quad (9)$$

which is the  $n$ -quantum spectral density function (i.e., the Fourier transform of the (auto)correlation function describing stochastic fluctuations in the local electromagnetic field that “relax” the probe's spin) characterized by an (exponential)<sup>110</sup> correlation time  $\tau_c$ .<sup>111</sup> Note that while Equation (9) is among the simplest forms for  $J_n$ , most reasonable choices for the (auto)correlation function yield similar results (see e.g.,<sup>112</sup>). In fact, the validity of this formulation of heteronuclear dipole-dipole SLR has been confirmed quantitatively in a previous  $\beta$ -NMR experiment on dilute  $^8\text{Li}$  in (isotopically pure)  $^7\text{Li}$  metal.<sup>113</sup>

In Equations (8) and (9), the connection to the local magnetic

where  $c$  is the slope of the linear relation. This does not, however, account for the finite intercept at  $T = 0$  K, which must find another origin such as the  $1/T_1^d$ , considered below.

The SLR term  $1/T_1^d$  accounts for relaxation resulting from magnetic fluctuations due to dipole-like fields in the vicinity of the probe. While the interaction is sensitive to the local field, it is sufficiently decoupled by typical NMR fields ( $> 1$  T) such that its contribution to SLR is often minor. Instead, the static (i.e., time-averaged) component of the dipole-dipole interaction is often the main observable, dictating the intrinsic width of the NMR line.<sup>103</sup> Outside of this “high field” limit, however, both this quantity<sup>104</sup> and the SLR rate become field-dependent, the latter often becoming dominant in  $^8\text{Li}$   $\beta$ -NMR (see e.g.,<sup>53,55,56,76,77,105</sup>). This contribution to the SLR can be considered as a form of “cross-relaxation” with the host  $^{93}\text{Nb}$  nuclear spins ( $I = 9/2$ ;  $\gamma/(2\pi) = 10.4523(5)$  MHz  $\text{T}^{-1}$ ; 100% abundance),<sup>106</sup> whose dynamic behavior is stochastic with characteristic time-constants  $T_1$  and  $T_2$  for their longitudinal and transverse components, respectively (the latter being of greatest importance here). In essence, the polarization of the  $^8\text{Li}$  probes “leaks” into the  $^{93}\text{Nb}$  spin “bath” at a rate  $1/T_1^d$ . This process is strongly suppressed by large magnetic fields, except near (avoided) level-crossings in the eigenstates of the coupled spin system (see e.g.,<sup>55,107</sup>) or at low magnetic fields where it dominates<sup>108</sup>. In fact, cross-relaxation between  $^8\text{Li}$  and  $^{93}\text{Nb}$  nuclei has been studied previously using (neutron activated)  $^8\text{Li}$   $\beta$ -NMR of  $\text{LiNbO}_3$ .<sup>107</sup>

Qualitatively, the SLR behavior of this cross-relaxation process can be described by a Lorentzian-like expression, with  $1/T_1^d \propto B^{-2}$  (see e.g.,<sup>53,55,56,76,77,105</sup>). Recognizing that our  $^8\text{Li}$  probe is unlike any of the “host”  $^{93}\text{Nb}$  spins, it is possible to describe their interaction more rigorously. Explicitly, for a probe spin  $I$  coupled to a lattice spin  $S$ , the heteronuclear dipole-dipole contribution to the SLR rate can be written as:<sup>34</sup>

$$\frac{1}{T_1^d} = \frac{1}{3} S(S+1) \langle \delta B_d^2 \rangle \left\{ \frac{1}{3} J_0(\omega_S - \omega_I) + J_1(\omega_I) + 2J_2(\omega_S + \omega_I) \right\}, \quad (8)$$

field is through the Larmor relation:

$$\omega_i = \gamma_i B(z), \quad (10)$$

where  $\gamma_i$  is the gyromagnetic ratio of the  $i^{\text{th}}$  nuclear spin, and  $B(z)$  is the local field, written suggestively to emphasize its spatial (i.e., depth) dependence. With Equation (10) providing the connection between the SLR rate [via Equations (8) and (9)] and the local field, we now consider the details of the latter.

In the normal state (i.e., when  $T > T_c$ ), there is no meaningful depth-dependence and  $B(z) = B_0$ , the applied magnetic field. In the limit that  $\tau_c$  is temperature-independent, Equation (8) reduces to a constant, equivalent to the non-zero  $1/T_1$  at 0 K (i.e., a finite intercept) the we infer from extrapolating our data. By contrast, in the Meissner state the local field is expected to be a strong function of  $z$  and we ascribe the

$E$ -dependence of our data to this fact. A salient feature of a superconductor in the Meissner state is the complete expulsion of magnetic flux from its interior. This is achieved by supercurrents within the material counter-acting the external field, causing it to “decay” over very short distances below the material’s surface (on the order of  $\sim 10$  nm to  $\sim 100$  nm). Quite generally, the screening of the magnetic field can be written as:<sup>16,17,58</sup>

$$B(z) = B_0 \left( \frac{2}{\pi} \right) \int_0^\infty \frac{q}{q^2 + K(q)} \sin(qz) dq, \quad (11)$$

where  $B_0$  is the applied field,  $z$  is the depth below the surface, and  $K(q)$  is the Fourier transform of the integrand kernel relating the current density  $\mathbf{j}$  to the vector potential  $\mathbf{A}$  inside a superconductor (see e.g.,<sup>19</sup>). In the absence of any appreciable dependence on the wavevector  $q$ ,  $K(q) \approx 1/\lambda^2$  and Equation (11) reduces to:

$$B(z) = B_0 \exp\left(-\frac{z}{\lambda}\right),$$

which is the famous (phenomenological) result of the London brothers.<sup>57</sup> A similar calculation, accounting for the boundary conditions specific to a film with thickness  $\zeta$ , as well as a non-superconducting “dead layer”  $d$  at the material’s surface (see e.g.,<sup>22</sup>), yields:<sup>58</sup>

$$B(z) = B_0 \times \begin{cases} 1, & z \leq d, \\ \frac{\cosh[(\zeta/2 - z - d)/\lambda]}{\cosh[\zeta/(2\lambda)]}, & d < z \leq \zeta. \end{cases} \quad (12)$$

We note that Equation (12) assumes no contribution from non-local electrodynamics.<sup>16,17,19</sup> Though non-local effects are expected to be present in “clean” Nb,<sup>19</sup> they are known to be weak and, as is shown below, they can be safely neglected.

While Equations (8) to (10) and (12) define the connection between the SLR rate and the spatial dependence of  $B$ , these alone cannot account for the temperature dependence in  $1/T_1$  that we observe. To reconcile this deficiency, it is necessary to also consider the temperature dependence of the penetration depth  $\lambda$ . Typically,  $\lambda$  is nearly temperature-independent when  $T \ll T_c$ , but diverges such that  $\lim_{T \rightarrow T_c} \lambda(T) = +\infty$ . While this behavior arises naturally from Equation (11) in the Bardeen-Cooper-Schrieffer (BCS) formulation of  $K(q)$ ,<sup>17</sup> the expressions are computationally cumbersome,<sup>19</sup> and we instead adopt the empirical “two-fluid” expression to describe the temperature dependence:

$$\lambda(T) = \begin{cases} \frac{\lambda_0}{\sqrt{1 - (T/T_c)^4}}, & T < T_c, \\ +\infty, & T \geq T_c, \end{cases} \quad (13)$$

where  $\lambda_0$  is the penetration depth at 0 K. We note that Equation (13) has been shown previously to accurately capture the temperature dependence of  $\lambda(T)$  in Nb.<sup>19</sup>

While these details can correctly explain the majority of our observations about the data, a remaining feature requiring explanation is the upturn in  $1/T_1$  observed at low- $T$  and low- $E$ .

At these  $E$  ( $< 2.5$  keV), we expect a substantial fraction of the implanted  $^8\text{Li}^+$  stop within the first  $\sim 5$  nm of the surface (see Figure 1), where a native oxide layer (e.g.,  $\text{Nb}_2\text{O}_5$ ) resides.<sup>71</sup> In the bulk, these oxides are known to be paramagnetic (e.g., due to oxygen sub-stoichiometry),<sup>90</sup> and this magnetism has been observed at the surface of Nb.<sup>91,114,115</sup> This leads us to postulate that the upturn is due to fluctuations in these electronic moments localized in the surface oxide layer. Noting that the upturn is appreciable at 3.5 K, but negligible at 11.9 K (see Figure 3), this SLR mechanism must be highly temperature dependent, with the fluctuation spectrum “freezing” into the vicinity of  $^8\text{Li}^+$ ’s Larmor frequency within a narrow temperature range. While this process can be described, in general, by a formalism analogous to that in Equations (8) and (9), our data is too limited for such a treatment and we instead adopt an additional power law term for stopping depths less than  $\sim 5$  nm:

$$\frac{1}{T_1^p} \approx \frac{C}{T^b}, \quad (14)$$

where  $b$  is the exponent and  $C$  is a constant. As is shown below, this gives a reasonable description of our data.

Based on the above discussion, we propose the following hierarchy to the SLR rates:

$$\frac{1}{T_1^q} < \frac{1}{T_1^e} \ll \frac{1}{T_1^l} \sim \frac{1}{T_1^p} \sim \frac{1}{T_1^d}.$$

We stress that only  $1/T_1^d$  can account for the SLR response observed upon transition from the normal to the Meissner state.<sup>53,56</sup> With these pieces in place, we now turn our attention to the  $^8\text{Li}^+$  stopping profile  $\rho(z; E)$  — the remaining “ingredient” required to evaluate Equation (4).

As mentioned in Section II,  $^8\text{Li}^+$  stopping profiles can be simulated reliably using Monte Carlo codes (e.g., SRIM<sup>68,69</sup>), producing histograms to represent  $\rho(z; E)$  (see Figure 1). For our analysis, it was convenient to have the ability to describe these profiles at *arbitrary*  $E$ , which can be accomplished by fitting the simulated profiles and interpolating their “shape” parameters. Empirically, we found that  $\rho(z; E)$  at a given  $E$  can be described, in general, by:

$$\rho(z; E) = \sum_i^n f_i p_i(z), \quad (15)$$

where  $p_i(z)$  is a probability density function,  $f_i \in [0, 1]$  is the  $i^{\text{th}}$  stopping fraction, constrained such that

$$\sum_i^n f_i \equiv 1,$$

and  $z$  is the depth below the surface. For our  $\text{Nb}_2\text{O}_5(5 \text{ nm})/\text{Nb}$  target (see e.g.,<sup>71</sup>), the stopping data are well-described using  $n = 2$  and a  $p(z)$  given by a modified beta distribution.<sup>116</sup> Explicitly,

$$p(z) = \begin{cases} 0, & z < 0 \\ \frac{(z/z_0)^{\alpha-1} (1 - z/z_0)^{\beta-1}}{z_0 B(\alpha, \beta)}, & 0 \leq z \leq z_0 \\ 0, & z > z_0 \end{cases} \quad (16)$$

where  $z \in [0, z_0]$  is the depth below the surface and  $B(\alpha, \beta)$  is the beta function:

$$B(\alpha, \beta) \equiv \frac{\Gamma(\alpha)\Gamma(\beta)}{\Gamma(\alpha + \beta)},$$

with  $\Gamma(s)$  denoting the gamma function:

$$\Gamma(s) \equiv \int_0^\infty x^{s-1} \exp(-x) dx.$$

Note that the “extra”  $z_0$  in the denominator of Equation (16) ensures proper normalization of  $p(z)$ . This (phenomenological) parameterization of the  $^8\text{Li}^+$  stopping profiles was found to work well for  $E \leq 30$  keV and a subset of the fit results are shown in Figure 1.

With all the pieces now in hand, we briefly summarize the most important details of our  $1/T_1$  model. The major SLR term  $1/T_{1d}$  [Equations (8) and (9)] has a field dependence of the form:

$$1/T_{1d} \propto 1/(1 + \zeta B^2),$$

where  $\zeta$  is a scalar value. Above  $T_c$ ,  $B$  is equal to the external field and is independent of  $^8\text{Li}$ 's position  $z$  below Nb's surface, resulting in a constant  $1/T_{1d}$ . Below  $T_c$ , the local magnetic field in Nb decreases as  $z$  approaches the film's center [Equation (12)] due to the Meissner effect, causing the spatially averaged  $1/T_{1d}$  to increase with decreasing temperature. This change is abrupt, occurring immediately below  $T_c$ , where the penetration depth  $\lambda$  changes rapidly [Equation (13)]. At lower temperatures,  $\lambda$  approaches a constant value and so too does  $1/T_{1d}$ . Similarly, as the implantation energy  $E$  is increased, the implanted  $^8\text{Li}$  sample depths closer to the film's center (see Figure 1) where the local field is lowest, causing the spatially averaged  $1/T_{1d}$  to increase with increasing implantation energy (up to the maximum  $E$  of 20 keV used here).

Finally, with these details in mind, it is straightforward to construct a model to describe the  $1/T_1$  data for Nb in Figure 3. Explicitly, a full three-dimensional (3D) fit (i.e.,  $1/T_1$  vs.  $E$ ,  $T$ , and  $B$ ) was performed by: combining Equations (7) to (10) and (12) to (14) into an expression for  $1/T_1(z)$ ; parameterizing  $\rho(z; E)$  using Equations (15) and (16) and interpolating their “shape” parameters; plugging these expressions into Equation (4) and evaluating the integral numerically<sup>117</sup>. The fit included *all* experimental data below 15 K<sup>118</sup>, and the result is shown in Figure 3. A summary of the main fit parameters determined from this procedure is given in Table I.

#### IV. DISCUSSION

It is clear from Figure 3 that our model for the  $^8\text{Li}$   $1/T_1$  (described in Section III C) is able to accurately reproduce our SLR data in the Nb film. Such good agreement is a strong confirmation of the choices made throughout our analysis. To further contextualize the results, we now consider the extracted parameters explicitly.

We shall start our discussion with the film's critical temperature  $T_c = 8.775(14)$  K, which is slightly below its “bulk”

value of  $\sim 8.9$  K determined from magnetometry. This difference, however, is consistent with the well-known suppression of  $T_c$  by an applied field and its small uncertainty emphasizes that it is well-defined by our model. This has bearing on  $\lambda(T)$ , whose temperature dependence is defined by Equation (13). This expression's other term of consequence, the magnetic penetration depth at 0 K  $\lambda_0$ , was determined to be 51.5(22) nm. The magnitude of this value is common for Nb films (see e.g.,<sup>119–125</sup>) and larger than the so-called London penetration depth  $\lambda_L$  often quoted for bulk Nb (see below). Noting that our film is thick compared to Nb's BCS coherence length  $\xi_0 \approx 40$  nm (derived from an average of literature values<sup>1,119,120,122,126–132</sup>), this “discrepancy” can be understood not in terms of a finite-size effect,<sup>125</sup> but rather in terms of the “dirty”<sup>58,133</sup> character of our film. It can be shown that, at 0 K, one obtains the simple relationship:<sup>58</sup>

$$\lambda_0 = \lambda_L \sqrt{1 + \frac{\xi_0}{\ell}}, \quad (17)$$

defining the influence of the carrier mean-free-path  $\ell$  on  $\lambda_0$ . Taking  $\lambda_L \approx 29$  nm (based on an average of literature values<sup>1,119–122,126–129,131,134–136</sup>), and re-arranging Equation (17), we obtain  $\ell = 18.7(29)$  nm, in good agreement with the range of values found in similarly prepared films (see e.g.,<sup>125,137–139</sup>). Within the Pippard<sup>16</sup> or BCS<sup>17</sup> theories, such a short  $\ell$  corresponds to an “effective” coherence length  $\xi \approx 13$  nm, placing the results firmly within the “local” regime (i.e., where  $\lambda > \xi > \ell$  — see e.g.,<sup>133</sup>). Note that, in this limit, accounting for non-local electrodynamics in the calculation of  $B(z)$ <sup>16,17</sup> is unnecessary, in contrast to that expected for “clean” Nb.<sup>19</sup>

We now turn our attention to the correlation time  $\tau_c = 6.1(5) \times 10^{-6}$  s of the fluctuations causing the  $^8\text{Li}$  SLR. We remark that this value is larger by a factor of  $\sim 10$  than the quantity derived from the  $\sim 0.2$  T “width” of the Lorentzian field-dependence quoted for earlier measurements at 10 K and higher fields.<sup>76</sup> We emphasize that, though not explicitly discussed in Ref. 76, the field-dependence is a manifestation of the cross-relaxation discussed in Section III C. It should be remarked, however, that differences in the two quantities are expected, for example, due to the orientation dependence of spectral densities (see e.g.,<sup>33–35</sup>). While the earlier estimate was made using a limited set of measurements,<sup>76</sup> our value is derived using both a more comprehensive dataset and a more accurate model for the field dependence,<sup>34,113</sup> suggesting that is the more reliable quantity. This is confirmed by its close proximity to the  $^{93}\text{Nb}$  spin-spin relaxation (SSR) time  $T_2 \approx 24 \mu\text{s}$ ,<sup>140</sup> differing from  $\tau_c$  by only a factor of  $\sim 4$ . Such a level of agreement is remarkable given the (indirect) manner in which  $\tau_c$  is identified. We also note that similar behavior has been observed for the low-field  $^8\text{Li}$  SLR in  $\text{Bi}_2\text{Te}_2\text{Se}$ .<sup>101</sup> Interestingly, the  $\tau_c$  in the Nb film is substantially shorter than in  $\text{NbSe}_2$ ,<sup>53</sup> presumably due to the reduced  $^{93}\text{Nb}$  spin density and  $^8\text{Li}$ 's weaker coupling to their fluctuations.

Next, we consider the “coupling” term in Equation (8): the dipolar field  $B_d = 41.1(21) \mu\text{T}$ . Interestingly, this value is a factor of  $\sim 10$  smaller than estimates obtained from lattice sums<sup>103</sup> for several plausible interstitial sites in Nb's BCC lattice,<sup>97</sup> as well as the  $^8\text{Li}$  resonance linewidths, both reported

previously.<sup>76</sup> This level of difference isn't unexpected, as the  $B_d$  in Equation (8) is a *dynamic* (i.e., fluctuating) quantity, which need not be similar in magnitude to its *static* (i.e., time-averaged) counterpart. In fact, this level difference is comparable to the case of  $^8\text{Li}$  in Cu, where estimates of  $B_d$  from detailed measurements of  $1/T_1$  in the vicinity of avoided level crossings (ALCs)<sup>55</sup> are an order of magnitude smaller than those inferred from lattice sums<sup>141</sup> and resonance linewidths.<sup>141,142</sup> We stress that  $1/T_1$  ALC measurements should provide the most accurate determination of  $B_d$ ; however, much like the use of lattice sums<sup>103,104</sup> they require a structural model of the  $^8\text{Li}^+$  site in the host material. While we do not have an independent experimental verification of our  $B_d$  at this time, we suggest that its value is reasonable. Key to verifying this hypothesis will be developing a detailed understanding of the  $^8\text{Li}^+$  defect site using quantum chemical models. Current information from high-field  $\beta$ -NMR experiments<sup>76</sup> and preliminary DFT calculations<sup>82</sup> suggest that a Li–Nb dumbbell-like defect complex is formed at the low temperatures employed in these experiments.

The next quantity to discuss is the slope of the linear term  $c = 0.697(11) \text{ s}^{-1} \text{ K}^{-1}$  in Equation (7). There is some difficulty interpreting this value. First, we reiterate that this is *not* due to a Korringa mechanism,<sup>35,89</sup> whose slope is orders of magnitude smaller<sup>76</sup> (see also Section III C). The stark difference in these quantities implies that  $c$  is highly dependent on  $B_0$ , though the precise mechanism is unclear (e.g., fluctuations in the *longitudinal* component of the Nb spin-system). At the level of empiricism, this behavior has also been observed in the  $^8\text{Li}$   $\beta$ -NMR of other metallic systems, including: Au,<sup>77,105</sup> Cu,<sup>55</sup> NbSe<sub>2</sub>,<sup>53</sup> and Bi<sub>2</sub>Ch<sub>3</sub> (Ch = Se, Te).<sup>101,102</sup> For the latter materials, it was suggested that the change in  $c$  may be related to charge-carrier-freezing in an applied field (see e.g.,<sup>143–145</sup>); however, its applicability to our elemental metal seems minimal. Alternatively, the behavior in NbSe<sub>2</sub> was thought to be due to fluctuations in the  $^{93}\text{Nb}$   $T_1$ ,<sup>53</sup> based on reasonable agreement between the estimated  $\tau_c$  and the  $1/e$  decay time for the SLR in the nuclear quadrupole resonance (NQR) regime.<sup>146</sup> While this remains the most plausible explanation for the behavior in Nb, making an equivalent comparison is hampered by the unavailability of  $^{93}\text{Nb}$  SLR measurements at comparable fields (see e.g.,<sup>140,147,148</sup>). To be more conclusive, a systematic study of  $c(B)$  seems necessary. Such an investigation may be possible in the near future thanks to a newly developed  $\beta$ -NMR instrument designed to operate from 0 mT to 200 mT.<sup>149</sup>

Finally, we consider the parameterization of the near-surface behavior of  $1/T_1$ , namely, the upturn in SLR in the Meissner state at  $E < 2.5 \text{ keV}$  and the extent of the (non-superconducting) “dead layer”. We note that there is some ambiguity in quantifying these features, owing to the rather limited data at these implantation energies. Empirically, the low- $E$  increase in  $1/T_1$  can be described by the power law in Equation (14) with a fixed exponent  $b = 4.5$  and  $C = 2.03(19) \times 10^3 \text{ s}^{-1} \text{ K}^{4.5}$ . Note that it was not possible to identify unique solutions for  $C$ ,  $b$ , and  $d$  without fixing one of the parameters, due to their high degree of correlation. We are not aware of any physical significance for the value of our exponent  $b$  used in Equation (14), making the connection of

$C$  to the magnetic properties of Nb<sub>2</sub>O<sub>5-x</sub><sup>90</sup> unclear. While paramagnetism in Nb's surface oxide layer<sup>91,114,115</sup> remains the likely source, further measurements (e.g., in a Nb<sub>2</sub>O<sub>5</sub> film) are necessary to be conclusive. Despite these ambiguities, our model determined the superconducting “dead layer”  $d$  to be 5.0(9) nm for our film, in excellent agreement with the typical thickness of the oxide layer that forms natively at the surface of Nb.<sup>71</sup> While this value also compares well with LE- $\mu$ SR measurements on a similar film,<sup>19</sup> it is much smaller than typical values found in Nb prepared for SRF applications.<sup>20–22</sup> This difference is likely due to greater surface roughness in the SRF samples<sup>150</sup>, which is known to influence the extent of the “dead layer” (see e.g.,<sup>151–153</sup>). We emphasize though that this quantity is inherent to a given *sample*, rather than being intrinsic to the material. Further SLR measurements at low implantation energies, including their temperature dependence, are required for deeper insight.

## V. CONCLUSIONS

We used  $^8\text{Li}$   $\beta$ -NMR to measure the Meissner screening profile in Nb(300 nm)/Al<sub>2</sub>O<sub>3</sub> thin film. Expanding on an earlier characterization performed at high magnetic field,<sup>76</sup> we measured the SLR rate  $1/T_1$ 's dependence on temperature and  $^8\text{Li}^+$  implantation energy (i.e., depth below the surface), in an applied field of 20 mT (parallel to the film's surface). While measurements at constant temperature in the normal state showed no depth-dependence, the SLR rate was found to vary strongly with implantation energy, increasing deeper below the surface. These observations were complemented by temperature dependent measurements at constant implantation energy, showing a linear variation in the normal state ( $1/T_1 = 0.697(11) \text{ s}^{-1} \text{ K}^{-1} \times T$ ), but with a pronounced “kink” at  $T_c = 8.775(14) \text{ K}$  and a non-linear increase at lower temperatures where  $1/T_1 \propto B(z)^{-2}$ , consistent with the  $^8\text{Li}$  SLR in other superconductors.<sup>53,56</sup> From a fit of the data to a model accounting for these details and the  $^8\text{Li}^+$  stopping profile, it was found that the Meissner screening is well-described by a simple London model with a magnetic penetration depth  $\lambda_0 = 51.5(22) \text{ nm}$  (extrapolated to 0 K). The large  $\lambda_0$  compared to Nb's intrinsic London penetration depth  $\lambda_L \approx 29 \text{ nm}$  is consistent with a relatively short carrier mean-free-path  $\ell = 18.7(29) \text{ nm}$  often found in similarly prepared films.<sup>125,137–139</sup>

This work constitutes an important advance in the use of  $^8\text{Li}$   $\beta$ -NMR to study materials rich in (stable) nuclear spins at low magnetic fields. Similarly, it provides a basis for understanding and modelling the SLR response in other superconductors, where measurements in this field regime are likely required (i.e., to remain in the Meissner state). For the specific case of studying Nb, this work provides a foundation for analyzing and interpreting results in samples with *engineered* surfaces (e.g., from mild baking<sup>4,5</sup> or doping<sup>6,7</sup>), where  $\lambda$  may be spatially *inhomogeneous* (see e.g.,<sup>154–156</sup>). There is even further interest in extending this study to fields on the order of Nb's superheating field  $B_{\text{sh}} \sim 200 \text{ mT}$ ,<sup>157,158</sup> where SRF cavities typically operate. A new beamline and instrument have been developed

for this purpose<sup>149</sup> and the measurement programme is already underway.

## ACKNOWLEDGMENTS

We thank: R. Abasalti, D. J. Arseneau, S. Daviel, B. Hitti, and D. Vyas for their excellent technical support; as well as D. Fujimoto for useful discussions. This work was supported by Natural Sciences and Engineering Research Council of Canada (NSERC) Awards to: T. J., R. F. K., and W. A. M.

## AUTHOR DECLARATIONS

### Conflicts of Interests

The authors have no conflicts to disclose.

### Author Contributions

**Ryan M. L. McFadden:** Formal Analysis (lead); Investigation (equal); Software (lead); Visualization (lead); Writing — Original Draft Preparation (lead); Writing — Review & Editing (lead). **Md Asaduzzaman:** Formal Analysis (supporting). **Terry J. Buck:** Investigation (equal). **David L. Cortie:** Investigation (equal). **Martin H. Dehn:** Investigation (equal). **Sarah R. Dunsiger:** Investigation (equal). **Robert F. Kiefl:** Conceptualization (equal); Funding Acquisition (equal); Investigation (equal). Writing — Review & Editing (supporting). **Robert E. Laxdal:** Formal Analysis (supporting); Writing — Review & Editing (supporting). **C. D. Philip Levy:** Investigation (supporting); Resources (equal). **W. Andrew MacFarlane:** Conceptualization (equal); Funding Acquisition (equal); Investigation (equal); Writing — Review & Editing (supporting). **Gerald D. Morris:** Investigation (equal); Resources (equal). **Matthew R. Pearson:** Investigation (supporting); Resources (equal). **Edward Thoeng:** Formal Analysis (supporting); Writing — Review & Editing (supporting). **Tobias Junginger:** Formal Analysis (supporting); Funding Acquisition (equal); Writing — Review & Editing (supporting).

### Data Availability

Raw data from the  $\beta$ -NMR experiments were generated at TRIUMF's Centre for Molecular and Materials Science (CMMS) facility and are available for download from: <https://cmms.triumf.ca/>. Derived data supporting the findings of this study are available from the corresponding authors upon reasonable request.

<sup>1</sup>D. K. Finnemore, T. F. Stromberg, and C. A. Swenson, "Superconducting properties of high-purity niobium," *Phys. Rev.* **149**, 231–243 (1966).

<sup>2</sup>H. Padamsee, J. Knobloch, and T. Hays, *RF Superconductivity for Accelerators*, 2nd ed., Wiley Series in Beam Physics and Accelerator Technology (Wiley, New York, 2008).

<sup>3</sup>H. Padamsee, *RF Superconductivity: Science, Technology, and Applications* (Wiley, Weinheim, 2009).

<sup>4</sup>G. Ciovati, "Effect of low-temperature baking on the radio-frequency properties of niobium superconducting cavities for particle accelerators," *J. Appl. Phys.* **96**, 1591–1600 (2004).

<sup>5</sup>A. Grassellino, A. Romanenko, D. Bice, O. Melnychuk, A. C. Crawford, S. Chandrasekaran, Z. Sung, D. A. Sergatskov, M. Checchin, S. Posen, M. Martinello, and G. Wu, "Accelerating fields up to 49 MV m<sup>-1</sup> in TESLA-shape superconducting RF niobium cavities via 75 °C vacuum bake," [arXiv:1806.09824 \[physics.acc-ph\]](https://arxiv.org/abs/1806.09824).

<sup>6</sup>A. Grassellino, A. Romanenko, D. Sergatskov, O. Melnychuk, Y. Trenikhina, A. Crawford, A. Rowe, M. Wong, T. Khabiboulline, and F. Barkov, "Nitrogen and argon doping of niobium for superconducting radio frequency cavities: a pathway to highly efficient accelerating structures," *Supercond. Sci. Technol.* **26**, 102001 (2013).

<sup>7</sup>A. Grassellino, A. Romanenko, Y. Trenikhina, M. Checchin, M. Martinello, O. S. Melnychuk, S. Chandrasekaran, D. A. Sergatskov, S. Posen, A. C. Crawford, S. Aderhold, and D. Bice, "Unprecedented quality factors at accelerating gradients up to 45 MV m<sup>-1</sup> in niobium superconducting resonators via low temperature nitrogen infusion," *Supercond. Sci. Technol.* **30**, 094004 (2017).

<sup>8</sup>A. Gurevich, "Enhancement of rf breakdown field of superconductors by multilayer coating," *Appl. Phys. Lett.* **88**, 012511 (2006).

<sup>9</sup>T. Kubo, Y. Iwashita, and T. Saeki, "Radio-frequency electromagnetic field and vortex penetration in multilayered superconductors," *Appl. Phys. Lett.* **104**, 032603 (2014).

<sup>10</sup>A. Gurevich, "Maximum screening fields of superconducting multilayer structures," *AIP Adv.* **5**, 017112 (2015).

<sup>11</sup>S. Posen, M. K. Transtrum, G. Catelani, M. U. Liepe, and J. P. Sethna, "Shielding superconductors with thin films as applied to rf cavities for particle accelerators," *Phys. Rev. Appl.* **4**, 044019 (2015).

<sup>12</sup>T. Kubo, "Multilayer coating for higher accelerating fields in superconducting radio-frequency cavities: a review of theoretical aspects," *Supercond. Sci. Technol.* **30**, 023001 (2017).

<sup>13</sup>T. Kubo, "Optimum multilayer coating of superconducting particle accelerator cavities and effects of thickness dependent material properties of thin films," *Jpn. J. Appl. Phys.* **58**, 088001 (2019).

<sup>14</sup>P. Bakule and E. Morenzoni, "Generation and applications of slow polarized muons," *Contemp. Phys.* **45**, 203–225 (2004).

<sup>15</sup>A. D. Hillier, S. J. Blundell, I. McKenzie, I. Umegaki, L. Shu, J. A. Wright, T. Prokscha, F. Bert, K. Shimomura, A. Berlie, H. Alberto, and I. Watanabe, "Muon spin spectroscopy," *Nat. Rev. Methods Primers* **2**, 4 (2022).

<sup>16</sup>A. B. Pippard, "An experimental and theoretical study of the relation between magnetic field and current in a superconductor," *Proc. R. Soc. London A* **216**, 547–568 (1953).

<sup>17</sup>J. Bardeen, L. N. Cooper, and J. R. Schrieffer, "Theory of superconductivity," *Phys. Rev.* **108**, 1175–1204 (1957).

<sup>18</sup>S. B. Nam, "Theory of electromagnetic properties of superconducting and normal systems. I," *Phys. Rev.* **156**, 470–486 (1967).

<sup>19</sup>A. Suter, E. Morenzoni, N. Garifanov, R. Khasanov, E. Kirk, H. Luetkens, T. Prokscha, and M. Horisberger, "Observation of nonexponential magnetic penetration profiles in the Meissner state: A manifestation of nonlocal effects in superconductors," *Phys. Rev. B* **72**, 024506 (2005).

<sup>20</sup>T. Junginger, S. Calatroni, A. Sublet, G. Terenziani, T. Prokscha, Z. Salman, A. Suter, T. Proslir, and J. Zasadzinski, "A low energy muon spin rotation and point contact tunneling study of niobium films prepared for superconducting cavities," *Supercond. Sci. Technol.* **30**, 125013 (2017).

<sup>21</sup>A. Romanenko, A. Grassellino, F. Barkov, A. Suter, Z. Salman, and T. Prokscha, "Strong Meissner screening change in superconducting radio frequency cavities due to mild baking," *Appl. Phys. Lett.* **104**, 072601 (2014).

<sup>22</sup>R. M. L. McFadden, M. Asaduzzaman, T. Prokscha, Z. Salman, A. Suter, and T. Junginger, "Depth-resolved measurements of the Meissner screening profile in surface-treated Nb," *Phys. Rev. Appl.* **19**, 044018 (2023).

<sup>23</sup>R. M. L. McFadden, M. Asaduzzaman, and T. Junginger, "Comment on "Strong Meissner screening change in superconducting radio frequency cavities due to mild baking" [*Appl. Phys. Lett.* 104, 072601 (2014)]," [arXiv:2305.02129 \[cond-mat.supr-con\]](https://arxiv.org/abs/2305.02129).

<sup>24</sup>W. A. MacFarlane, "Implanted-ion  $\beta$ NMR: A new probe for nanoscience," *Solid State Nucl. Magn. Reson.* **68–69**, 1–12 (2015).

- <sup>25</sup>W. A. MacFarlane, "Status and progress of ion-implanted  $\beta$ NMR at TRIUMF," *Z. Phys. Chem.* **236**, 757–798 (2022).
- <sup>26</sup>H. Ackermann, P. Heitjans, and H.-J. Stöckmann, " $\beta$  emitters and isomeric nuclei as probes in condensed matter," in *Hyperfine Interactions of Radioactive Nuclei*, Topics in Current Physics, Vol. 31, edited by J. Christiansen (Springer, Berlin, 1983) Chap. 6, pp. 291–361.
- <sup>27</sup>W. Widdra, M. Detje, H. Ebinger, H. J. Jänsch, W. Preyss, H. Reich, R. Veith, D. Fick, M. Röckelein, and H. Völk, " $\beta$ -NMR on single-crystal surfaces: Method," *Rev. Sci. Instrum.* **66**, 2465–2475 (1995).
- <sup>28</sup>C. D. P. Levy, M. R. Pearson, R. F. Kiefl, E. Mané, G. D. Morris, and A. Voss, "Laser polarization facility," *Hyperfine Interact.* **225**, 165–172 (2014).
- <sup>29</sup>G. D. Morris, " $\beta$ -NMR," *Hyperfine Interact.* **225**, 173–182 (2014).
- <sup>30</sup>S. R. Kreitzman and G. D. Morris, "TRIUMF MuSR and  $\beta$ NMR research facilities," *JPS Conf. Proc.* **21**, 011056 (2018).
- <sup>31</sup>T. D. Lee and C. S. Wu, "Weak interactions," *Annu. Rev. Nucl. Sci.* **15**, 381–476 (1965).
- <sup>32</sup>E. Morenzoni, T. Prokscha, A. Suter, H. Luetkens, and R. Khasanov, "Nano-scale thin film investigations with slow polarized muons," *J. Phys.: Condens. Matter* **16**, S4583–S4601 (2004).
- <sup>33</sup>A. Abragam, *The Principles of Nuclear Magnetism*, International Series of Monographs on Physics, Vol. 32 (Oxford University Press, Oxford, 1961).
- <sup>34</sup>M. Mehring, *Principles of High Resolution NMR in Solids*, 2nd ed. (Springer, Berlin, 1983).
- <sup>35</sup>C. P. Slichter, *Principles of Magnetic Resonance*, 3rd ed., Springer Series in Solid-State Sciences, Vol. 1 (Springer, Berlin, 1990).
- <sup>36</sup>A. J. Pell, G. Pintacuda, and C. P. Grey, "Paramagnetic NMR in solution and the solid state," *Prog. Nucl. Magn. Reson. Spectrosc.* **111**, 1–271 (2019).
- <sup>37</sup>T. J. Parolin, Z. Salman, J. Chakhalian, Q. Song, K. H. Chow, M. D. Hossain, T. A. Keeler, R. F. Kiefl, S. R. Kreitzman, C. D. P. Levy, R. I. Miller, G. D. Morris, M. R. Pearson, H. Saadaoui, D. Wang, and W. A. MacFarlane, " $\beta$ -NMR of isolated lithium in nearly ferromagnetic palladium," *Phys. Rev. Lett.* **98**, 047601 (2007).
- <sup>38</sup>Q. Song, K. H. Chow, Z. Salman, H. Saadaoui, M. D. Hossain, R. F. Kiefl, G. D. Morris, C. D. P. Levy, M. R. Pearson, T. J. Parolin, I. Fan, T. A. Keeler, M. Smadella, D. Wang, K. M. Yu, X. Liu, J. K. Furdyna, and W. A. MacFarlane, " $\beta$ -detected NMR of Li in  $\text{Ga}_{1-x}\text{Mn}_x\text{As}$ ," *Phys. Rev. B* **84**, 054414 (2011).
- <sup>39</sup>W. A. MacFarlane, T. J. Parolin, T. I. Larkin, G. Richter, K. H. Chow, M. D. Hossain, R. F. Kiefl, C. D. P. Levy, G. D. Morris, O. Ofer, M. R. Pearson, H. Saadaoui, Q. Song, and D. Wang, "Finite-size effects in the nuclear magnetic resonance of epitaxial palladium thin films," *Phys. Rev. B* **88**, 144424 (2013).
- <sup>40</sup>V. L. Karner, A. Chatzichristos, D. L. Cortie, M. H. Dehn, O. Foyevtsov, K. Foyevtsova, D. Fujimoto, R. F. Kiefl, C. D. P. Levy, R. Li, R. M. L. McFadden, G. D. Morris, M. R. Pearson, M. Stachura, J. O. Ticknor, G. Cristiani, G. Logvenov, F. Wrobel, B. Keimer, J. Zhang, J. F. Mitchell, and W. A. MacFarlane, "Local metallic and structural properties of the strongly correlated metal  $\text{LaNiO}_3$  using  $^8\text{Li}$   $\beta$ -NMR," *Phys. Rev. B* **100**, 165109 (2019).
- <sup>41</sup>T. A. Keeler, Z. Salman, K. H. Chow, B. Heinrich, M. D. Hossain, B. Kardasz, R. F. Kiefl, S. R. Kreitzman, C. D. P. Levy, W. A. MacFarlane, O. Mosendz, T. J. Parolin, M. R. Pearson, and D. Wang, "Hyperfine fields in an Ag/Fe multilayer film investigated with  $^8\text{Li}$   $\beta$ -detected NMR," *Phys. Rev. B* **77**, 144429 (2008).
- <sup>42</sup>Z. Salman, O. Ofer, M. Radovic, H. Hao, M. Ben Shalom, K. H. Chow, Y. Dagan, M. D. Hossain, C. D. P. Levy, W. A. MacFarlane, G. D. Morris, L. Patthey, M. R. Pearson, H. Saadaoui, T. Schmitt, D. Wang, and R. F. Kiefl, "Nature of weak magnetism in  $\text{SrTiO}_3/\text{LaAlO}_3$  multilayers," *Phys. Rev. Lett.* **109**, 257207 (2012).
- <sup>43</sup>W. A. MacFarlane, Q. Song, N. J. C. Ingle, K. H. Chow, M. Egilmez, I. Fan, M. D. Hossain, R. F. Kiefl, C. D. P. Levy, G. D. Morris, T. J. Parolin, M. R. Pearson, H. Saadaoui, Z. Salman, and D. Wang, " $\beta$ -detected NMR spin relaxation in a thin film heterostructure of ferromagnetic  $\text{EuO}$ ," *Phys. Rev. B* **92**, 064409 (2015).
- <sup>44</sup>V. L. Karner, A. Chatzichristos, D. L. Cortie, D. Fujimoto, R. F. Kiefl, C. D. P. Levy, R. Li, R. M. L. McFadden, G. D. Morris, M. R. Pearson, E. Benckiser, A. V. Boris, G. Cristiani, G. Logvenov, B. Keimer, and W. A. MacFarlane, "Evolution of the metallic state in  $\text{LaNiO}_3/\text{LaAlO}_3$  superlattices measured by  $^8\text{Li}$   $\beta$ -detected NMR," *Phys. Rev. B* **104**, 205114 (2021).
- <sup>45</sup>I. McKenzie, M. Harada, R. F. Kiefl, C. D. P. Levy, W. A. MacFarlane, G. D. Morris, S.-I. Ogata, M. R. Pearson, and J. Sugiyama, " $\beta$ -NMR measurements of lithium ion transport in thin films of pure and lithium-salt-doped poly(ethylene oxide)," *J. Am. Chem. Soc.* **136**, 7833–7836 (2014).
- <sup>46</sup>R. M. L. McFadden, T. J. Buck, A. Chatzichristos, C.-C. Chen, K. H. Chow, D. L. Cortie, M. H. Dehn, V. L. Karner, D. Koumoulis, C. D. P. Levy, C. Li, I. McKenzie, R. Merkle, G. D. Morris, M. R. Pearson, Z. Salman, D. Samuelis, M. Stachura, J. Xiao, J. Maier, R. F. Kiefl, and W. A. MacFarlane, "Microscopic dynamics of  $\text{Li}^+$  in rutile  $\text{TiO}_2$  revealed by  $^8\text{Li}$   $\beta$ -detected nuclear magnetic resonance," *Chem. Mater.* **29**, 10187–10197 (2017).
- <sup>47</sup>I. McKenzie, C. R. Daley, R. F. Kiefl, C. D. P. Levy, W. A. MacFarlane, G. D. Morris, M. R. Pearson, D. Wang, and J. A. Forrest, "Enhanced high-frequency molecular dynamics in the near-surface region of polystyrene thin films observed with  $\beta$ -NMR," *Soft Matter* **11**, 1755–1761 (2015).
- <sup>48</sup>I. McKenzie, Y. Chai, D. L. Cortie, J. A. Forrest, D. Fujimoto, V. L. Karner, R. F. Kiefl, C. D. P. Levy, W. A. MacFarlane, R. M. L. McFadden, G. D. Morris, M. R. Pearson, and S. Zhu, "Direct measurements of the temperature, depth and processing dependence of phenyl ring dynamics in polystyrene thin films by  $\beta$ -detected NMR," *Soft Matter* **14**, 7324–7334 (2018).
- <sup>49</sup>I. McKenzie, D. Fujimoto, V. L. Karner, R. Li, W. A. MacFarlane, R. M. L. McFadden, G. D. Morris, M. R. Pearson, A. N. Raegen, M. Stachura, J. O. Ticknor, and J. A. Forrest, "A  $\beta$ -NMR study of the depth, temperature, and molecular-weight dependence of secondary dynamics in polystyrene: Entropy–enthalpy compensation and dynamic gradients near the free surface," *J. Chem. Phys.* **156**, 084903 (2022).
- <sup>50</sup>Z. Salman, K. H. Chow, R. I. Miller, A. Morello, T. J. Parolin, M. D. Hossain, T. A. Keeler, C. D. P. Levy, W. A. MacFarlane, G. D. Morris, H. Saadaoui, D. Wang, R. Sessoli, G. G. Condorelli, and R. F. Kiefl, "Local magnetic properties of a monolayer of  $\text{Mn}_{12}$  single molecule magnets," *Nano Lett.* **7**, 1551–1555 (2007).
- <sup>51</sup>D. L. Cortie, T. Buck, M. H. Dehn, V. L. Karner, R. F. Kiefl, C. D. P. Levy, R. M. L. McFadden, G. D. Morris, I. McKenzie, M. R. Pearson, X. L. Wang, and W. A. MacFarlane, " $\beta$ -NMR investigation of the depth-dependent magnetic properties of an antiferromagnetic surface," *Phys. Rev. Lett.* **116**, 106103 (2016).
- <sup>52</sup>Z. Salman, D. Wang, K. H. Chow, M. D. Hossain, S. R. Kreitzman, T. A. Keeler, C. D. P. Levy, W. A. MacFarlane, R. I. Miller, G. D. Morris, T. J. Parolin, H. Saadaoui, M. Smadella, and R. F. Kiefl, "Magnetic-field effects on the size of vortices below the surface of  $\text{NbSe}_2$  detected using low energy  $\beta$ -NMR," *Phys. Rev. Lett.* **98**, 167001 (2007).
- <sup>53</sup>M. D. Hossain, Z. Salman, D. Wang, K. H. Chow, S. Kreitzman, T. A. Keeler, C. D. P. Levy, W. A. MacFarlane, R. I. Miller, G. D. Morris, T. J. Parolin, M. Pearson, H. Saadaoui, and R. F. Kiefl, "Low-field cross spin relaxation of  $^8\text{Li}$  in superconducting  $\text{NbSe}_2$ ," *Phys. Rev. B* **79**, 144518 (2009).
- <sup>54</sup>R. F. Kiefl, G. D. Morris, P. Amaudruz, R. Baartman, J. Behr, J. H. Brewer, J. Chakhalian, S. Daviel, J. Doornbos, S. Dunsiger, S. R. Kreitzman, T. Kuo, C. D. P. Levy, R. Miller, M. Olivo, R. Poutissou, G. W. Wright, and A. Zelenki, "Complementarity of low-energy spin polarized radioactive nuclei and muons," *Physica B* **289–290**, 640–647 (2000).
- <sup>55</sup>K. H. Chow, A. I. Mansour, I. Fan, R. F. Kiefl, G. D. Morris, Z. Salman, T. Dunlop, W. A. MacFarlane, H. Saadaoui, O. Mosendz, B. Kardasz, B. Heinrich, J. Jung, C. D. P. Levy, M. R. Pearson, T. J. Parolin, D. Wang, M. D. Hossain, Q. Song, and M. Smadella, "Detection and decoherence of level-crossing resonances of  $^8\text{Li}$  in Cu," *Phys. Rev. B* **85**, 092103 (2012).
- <sup>56</sup>E. Morenzoni, H. Saadaoui, D. Wang, M. Horisberger, E. C. Kirk, W. A. MacFarlane, G. D. Morris, K. H. Chow, M. D. Hossain, C. P. Levy, T. J. Parolin, M. R. Pearson, Q. Song, and R. F. Kiefl, "Slow order-parameter fluctuations in superconducting Pb and Ag/Nb films observed using  $\beta$ -detected nuclear magnetic resonance," *Phys. Rev. B* **85**, 220501 (2012).
- <sup>57</sup>F. London and H. London, "The electromagnetic equations of the superconductor," *Proc. R. Soc. London A* **149**, 71–88 (1935).
- <sup>58</sup>M. Tinkham, *Introduction to Superconductivity*, 2nd ed., International Series in Pure and Applied Physics (McGraw-Hill, New York, 1996).
- <sup>59</sup>N. J. Stone, "Table of recommended nuclear magnetic dipole moments: Part I — long-lived," 0794 (International Atomic Energy Agency, Vienna, 2019).
- <sup>60</sup>E. Tiesinga, P. J. Mohr, D. B. Newell, and B. N. Taylor, "CODATA recommended values of the fundamental physical constants: 2018," *Rev. Mod. Phys.* **93**, 025010 (2021).

- <sup>61</sup>N. J. Stone, “Table of nuclear electric quadrupole moments,” INDC(NDS) 0833 (International Atomic Energy Agency, Vienna, 2021).
- <sup>62</sup>X. Fléchar, E. Liénard, O. Naviliat-Cuncic, D. Rodríguez, M. A. G. Alvarez, G. Ban, B. Carniol, D. Etasse, J. M. Fontbonne, A. M. Lallena, and J. Praena, “Measurement of the  $^8\text{Li}$  half-life,” *Phys. Rev. C* **82**, 027309 (2010).
- <sup>63</sup>W. J. Huang, M. Wang, F. G. Kondev, G. Audi, and S. Naimi, “The AME 2020 atomic mass evaluation (I). evaluation of input data, and adjustment procedures,” *Chin. Phys. C* **45**, 030002 (2021).
- <sup>64</sup>M. Wang, W. J. Huang, F. G. Kondev, G. Audi, and S. Naimi, “The AME 2020 atomic mass evaluation (II). tables, graphs and references,” *Chin. Phys. C* **45**, 030003 (2021).
- <sup>65</sup>P. G. Bricault, F. Ames, M. Domsbky, P. Kunz, and J. Lassen, “Rare isotope beams at ISAC — target & ion source systems,” *Hyperfine Interact.* **225**, 25–49 (2014).
- <sup>66</sup>C. D. P. Levy, A. Hatakeyama, Y. Hirayama, R. F. Kiefl, R. Baartman, J. A. Behr, H. Izumi, D. Melconian, G. D. Morris, R. Nussbaumer, M. Olivo, M. Pearson, R. Poutissou, and G. W. Wight, “Polarized radioactive beam at ISAC,” *Nucl. Instrum. Methods Phys. Res., Sect. B* **204**, 689–693 (2003).
- <sup>67</sup>W. A. MacFarlane, C. D. P. Levy, M. R. Pearson, T. Buck, K. H. Chow, A. N. Hariwal, R. F. Kiefl, F. H. McGee, G. D. Morris, and D. Wang, “The initial state of optically polarized  $^8\text{Li}^+$  from the  $\beta$ -NMR in bismuth,” *J. Phys.: Conf. Ser.* **551**, 012059 (2014).
- <sup>68</sup>J. F. Ziegler, J. P. Biersack, and M. D. Ziegler, *SRIM — The Stopping and Range of Ions in Matter*, 7th ed. (SRIM Co., Chester, 2008).
- <sup>69</sup>J. F. Ziegler, M. D. Ziegler, and J. P. Biersack, “SRIM — the stopping and range of ions in matter (2010),” *Nucl. Instrum. Methods Phys. Res., Sect. B* **268**, 1818–1823 (2010).
- <sup>70</sup>C. Ostrouchov, Y. Zhang, and W. J. Weber, “pysrim: Automation, analysis, and plotting of SRIM calculations,” *J. Open Source Software* **3**, 829 (2018).
- <sup>71</sup>J. Halbritter, “On the oxidation and on the superconductivity of niobium,” *Appl. Phys. A* **43**, 1–28 (1987).
- <sup>72</sup>M. Nastasi and J. W. Mayer, *Ion Implantation and Synthesis of Materials* (Springer, Berlin, 2006).
- <sup>73</sup>W. Eckstein, *Computer Simulation of Ion-Solid Interactions*, Springer Series in Materials Science, Vol. 10 (Springer, Berlin, 1991).
- <sup>74</sup>E. Morenzoni, H. Glückler, T. Prokscha, R. Khasanov, H. Luetkens, M. Birke, E. M. Forgan, C. Niedermayer, and M. Pleines, “Implantation studies of keV positive muons in thin metallic layers,” *Nucl. Instrum. Methods Phys. Res., Sect. B* **192**, 254–266 (2002).
- <sup>75</sup>A. F. A. Simões, H. V. Alberto, R. C. Vilão, J. M. Gil, J. M. V. Cunha, M. A. Curado, P. M. P. Salomé, T. Prokscha, A. Suter, and Z. Salman, “Muon implantation experiments in films: Obtaining depth-resolved information,” *Rev. Sci. Instrum.* **91**, 023906 (2020).
- <sup>76</sup>T. J. Parolin, J. Shi, Z. Salman, K. H. Chow, P. Dosanjh, H. Saadaoui, Q. Song, M. D. Hossain, R. F. Kiefl, C. D. P. Levy, M. R. Pearson, and W. A. MacFarlane, “Nuclear magnetic resonance study of Li implanted in a thin film of niobium,” *Phys. Rev. B* **80**, 174109 (2009).
- <sup>77</sup>W. A. MacFarlane, K. H. Chow, M. D. Hossain, V. L. Karner, R. F. Kiefl, R. M. L. McFadden, G. D. Morris, H. Saadaoui, and Z. Salman, “The spin relaxation of  $^8\text{Li}^+$  in gold at low magnetic field,” *JPS Conf. Proc.* **21**, 011020 (2018).
- <sup>78</sup>H.-J. Stöckmann and P. Heitjans, “Low-temperature nuclear spin-lattice relaxation in glasses — homogeneous and inhomogeneous averaging,” *J. Non-Cryst. Solids* **66**, 501–509 (1984).
- <sup>79</sup>A. F. McDowell, “Magnetization-recovery curves for quadrupolar spins,” *J. Magn. Reson., Ser. A* **113**, 242–246 (1995).
- <sup>80</sup>P. S. Hubbard, “Nonexponential nuclear magnetic relaxation by quadrupole interactions,” *J. Chem. Phys.* **53**, 985–987 (1970).
- <sup>81</sup>K. D. Becker, “Nuclear magnetic relaxation induced by the dynamics of lattice defects in solids ( $I = 3/2$ ,  $I = 2$ , and  $I = 5/2$ ),” *Z. Naturforsch. A* **37**, 697–705 (1982).
- <sup>82</sup>J. A. Adelman *et al.*, Unpublished.
- <sup>83</sup>Based on information about the  $^8\text{Li}$  stopping site (inferred from its resonance),<sup>76</sup> a more fundamental analysis might use a discrete sum of exponentials for  $R(t, t')$ ;<sup>77</sup> however, we find the quality of the present data inadequate for such a treatment, which yields ill-defined fit parameters due to over-parameterization. This phenomenon is not unique to Nb and simplified relaxation functions have often been used to quantify the SLR in other “simple” cubic metals (see e.g.,<sup>24</sup>).
- <sup>84</sup>We stress that neither of these choices fundamentally altered the observed trends in  $1/T_1$  (see Figure 3).
- <sup>85</sup>H. Takahasi and M. Mori, “Double exponential formulas for numerical integration,” *Publ. RIMS, Kyoto Univ.* **9**, 721–741 (1974).
- <sup>86</sup>M. Mori and M. Sugihara, “The double-exponential transformation in numerical analysis,” *J. Comput. Appl. Math.* **127**, 287–296 (2001).
- <sup>87</sup>D. Fujimoto, “Digging into MUD with Python: muddy, bdata, and bfit,” [arXiv:2004.10395 \[physics.data-an\]](https://arxiv.org/abs/2004.10395).
- <sup>88</sup>D. Fujimoto, “bfit: A Python application for beta-detected NMR,” *J. Open Source Software* **6**, 3598 (2021).
- <sup>89</sup>J. Korringa, “Nuclear magnetic relaxation and resonance line shift in metals,” *Physica* **16**, 601–610 (1950).
- <sup>90</sup>R. J. Cava, B. Batlogg, J. J. Krajewski, H. F. Poulsen, P. Gammel, W. F. Peck, and L. W. Rupp, “Electrical and magnetic properties of  $\text{Nb}_2\text{O}_{5-\delta}$  crystallographic shear structures,” *Phys. Rev. B* **44**, 6973–6981 (1991).
- <sup>91</sup>T. Proslir, M. Kharitonov, M. Pellin, J. Zasadzinski, and G. Ciovati, “Evidence of surface paramagnetism in niobium and consequences for the superconducting cavity surface impedance,” *IEEE Trans. Appl. Supercond.* **21**, 2619–2622 (2011).
- <sup>92</sup>R. L. Workman *et al.* (Particle Data Group), “Review of particle physics,” *Prog. Theor. Exp. Phys.* **2022**, 083C01 (2022).
- <sup>93</sup>W. A. MacFarlane *et al.*, Unpublished.
- <sup>94</sup>Note that the upper integration limit in Equation (4) is justified by the fact that  $\rho(z; E) \rightarrow 0$  for sufficiently large  $z$ .
- <sup>95</sup>Assuming the fluctuations are statistically independent.
- <sup>96</sup>This is also consistent with the absence of a Hebel-Slichter coherence peak<sup>159</sup> in the  $1/T_1$  data.
- <sup>97</sup>D. N. Beshers, “An investigation of interstitial sites in the bcc lattice,” *J. Appl. Phys.* **36**, 290–300 (1965).
- <sup>98</sup>W. A. MacFarlane, C. B. L. Tschense, T. Buck, K. H. Chow, D. L. Cortie, A. N. Hariwal, R. F. Kiefl, D. Koumoullis, C. D. P. Levy, I. McKenzie, F. H. McGee, G. D. Morris, M. R. Pearson, Q. Song, D. Wang, Y. S. Hor, and R. J. Cava, “ $\beta$ -detected NMR of  $^8\text{Li}^+$  in Bi, Sb, and the topological insulator  $\text{Bi}_{10.9}\text{Sb}_{0.1}$ ,” *Phys. Rev. B* **90**, 214422 (2014).
- <sup>99</sup>J. Van Kranendonk, “Theory of quadrupolar nuclear spin-lattice relaxation,” *Physica* **20**, 781–800 (1954).
- <sup>100</sup>In principle, this could be tested explicitly through a comparison of the  $^8\text{Li}$  and  $^9\text{Li}$  SLR rates (see e.g.,<sup>160</sup>).
- <sup>101</sup>R. M. L. McFadden, A. Chatzichristos, K. H. Chow, D. L. Cortie, M. H. Dehn, D. Fujimoto, M. D. Hossain, H. Ji, V. L. Karner, R. F. Kiefl, C. D. P. Levy, R. Li, I. McKenzie, G. D. Morris, O. Ofer, M. R. Pearson, M. Stachura, R. J. Cava, and W. A. MacFarlane, “Ionic and electronic properties of the topological insulator  $\text{Bi}_2\text{Te}_2\text{Se}$  investigated via  $\beta$ -detected nuclear magnetic relaxation and resonance of  $^8\text{Li}^+$ ,” *Phys. Rev. B* **99**, 125201 (2019).
- <sup>102</sup>R. M. L. McFadden, A. Chatzichristos, D. L. Cortie, D. Fujimoto, Y. S. Hor, H. Ji, V. L. Karner, R. F. Kiefl, C. D. P. Levy, R. Li, I. McKenzie, G. D. Morris, M. R. Pearson, M. Stachura, R. J. Cava, and W. A. MacFarlane, “Local electronic and magnetic properties of the doped topological insulators  $\text{Bi}_2\text{Se}_3\text{:Ca}$  and  $\text{Bi}_2\text{Te}_3\text{:Mn}$  investigated using ion-implanted  $^8\text{Li}$   $\beta$ -NMR,” *Phys. Rev. B* **102**, 235206 (2020).
- <sup>103</sup>J. H. Van Vleck, “The dipolar broadening of magnetic resonance lines in crystals,” *Phys. Rev.* **74**, 1168–1183 (1948).
- <sup>104</sup>O. Hartmann, “Quadrupole influence on the dipolar-field width for a single interstitial in a metal crystal,” *Phys. Rev. Lett.* **39**, 832–835 (1977).
- <sup>105</sup>T. J. Parolin, Z. Salman, K. H. Chow, Q. Song, J. Valiani, H. Saadaoui, A. O’Halloran, M. D. Hossain, T. A. Keeler, R. F. Kiefl, S. R. Kreitzman, C. D. P. Levy, R. I. Miller, G. D. Morris, M. R. Pearson, M. Smadella, D. Wang, M. Xu, and W. A. MacFarlane, “High resolution  $\beta$ -NMR study of  $^8\text{Li}^+$  implanted in gold,” *Phys. Rev. B* **77**, 214107 (2008).
- <sup>106</sup>C. M. Baglin, “Nuclear data sheets for  $A = 93$ ,” *Nucl. Data Sheets* **112**, 1163–1389 (2011).
- <sup>107</sup>F. Fujara, H.-J. Stöckmann, H. Ackermann, W. Buttler, K. Dörr, H. Grupp, P. Heitjans, G. Kiese, and A. Körblein, “Cross-relaxation processes of polarized  $\beta$ -active nuclei in various crystalline solids,” *Z. Phys. B: Condens. Matter* **37**, 151–161 (1980).
- <sup>108</sup>Alternatively, one may consider the low-field behavior as a form of avoided level-crossing resonance, with the “universal” resonance occurring at zero

- magnetic field.
- <sup>109</sup>Note that the magnitude of  $\langle \delta B_d^2 \rangle$  is dependent on the  $^8\text{Li}$  lattice site. Similarly, in environments where the inter-nuclear orientation is fixed (e.g., crystalline solids), it also depends on the applied field direction (see e.g., <sup>33–35</sup>).
- <sup>110</sup>This assumes that the  $^{93}\text{Nb}$  spins have adopted a single spin temperature.
- <sup>111</sup>N. Bloembergen, E. M. Purcell, and R. V. Pound, “Relaxation effects in nuclear magnetic resonance absorption,” *Phys. Rev.* **73**, 679–712 (1948).
- <sup>112</sup>P. A. Beckmann, “Spectral densities and nuclear spin relaxation in solids,” *Phys. Rep.* **171**, 85–128 (1988).
- <sup>113</sup>P. Heitjans, A. Körblein, H. Ackermann, D. Dubbers, F. Fujara, and H.-J. Stöckmann, “Self-diffusion in solid lithium probed by spin-lattice relaxation of  $^8\text{Li}$  nuclei,” *J. Phys. F: Met. Phys.* **15**, 41–54 (1985).
- <sup>114</sup>S. Casalbuoni, E. Knabbe, J. Kötzler, L. Lilje, L. von Sawilski, P. Schmäser, and B. Steffen, “Surface superconductivity in niobium for superconducting RF cavities,” *Nucl. Instrum. Methods Phys. Res., Sect. A* **538**, 45–64 (2005).
- <sup>115</sup>A. S. Samsonova, P. I. Zolotov, E. M. Baeva, A. I. Lomakin, N. A. Titova, A. I. Kardakova, and G. N. Goltsman, “Signatures of surface magnetic disorder in niobium films,” *IEEE Trans. Appl. Supercond.* **31**, 7000205 (2021).
- <sup>116</sup>A. K. Gupta and S. Nadarajah, eds., *Handbook of Beta Distribution and Its Applications* (CRC Press, Boca Raton, 2004).
- <sup>117</sup>Note that, for the numeric evaluation of Equation (4), both adaptive Gaussian<sup>161</sup> and tanh-sinh<sup>85,86</sup> quadrature were found to work well.
- <sup>118</sup>This restriction ensures that the approximation in Equation (7) holds; at higher temperatures the linear relation will likely break down due to  $^8\text{Li}$  undergoing a site-change-transition (see<sup>76</sup>).
- <sup>119</sup>P. W. Epperlein, “Magnetic penetration depths in superconducting Nb films,” *Physica B+C* **108**, 931–932 (1981).
- <sup>120</sup>A. Andreone, A. Cassinese, M. Iavarone, R. Vaglio, I. I. Kulik, and V. Palmieri, “Relation between normal-state and superconductive properties of niobium sputtered films,” *Phys. Rev. B* **52**, 4473–4476 (1995).
- <sup>121</sup>H. Zhang, J. W. Lynn, C. F. Majkrzak, S. K. Satija, J. H. Kang, and X. D. Wu, “Measurements of magnetic screening lengths in superconducting Nb thin films by polarized neutron reflectometry,” *Phys. Rev. B* **52**, 10395–10404 (1995).
- <sup>122</sup>A. V. Pronin, M. Dressel, A. Pimenov, A. Loidl, I. V. Roshchin, and L. H. Greene, “Direct observation of the superconducting energy gap developing in the conductivity spectra of niobium,” *Phys. Rev. B* **57**, 14416–14421 (1998).
- <sup>123</sup>A. I. Gubin, K. S. Il’in, S. A. Vitusevich, M. Siegel, and N. Klein, “Dependence of magnetic penetration depth on the thickness of superconducting Nb thin films,” *Phys. Rev. B* **72**, 064503 (2005).
- <sup>124</sup>E. Nazaretski, J. P. Thibodaux, I. Vekhter, L. Civale, J. D. Thompson, and R. Movshovich, “Direct measurements of the penetration depth in a superconducting film using magnetic force microscopy,” *Appl. Phys. Lett.* **95**, 262502 (2009).
- <sup>125</sup>N. Pinto, S. J. Rezvani, A. Perali, L. Flammia, M. V. Milošević, M. Fretto, C. Cassiago, and N. De Leo, “Dimensional crossover and incipient quantum size effects in superconducting niobium nanofilms,” *Sci. Rep.* **8**, 4710 (2018).
- <sup>126</sup>B. W. Maxfield and W. L. McLean, “Superconducting penetration depth of niobium,” *Phys. Rev.* **139**, A1515–A1522 (1965).
- <sup>127</sup>R. A. French, “Intrinsic type-2 superconductivity in pure niobium,” *Cryog.* **8**, 301–308 (1968).
- <sup>128</sup>J. Auer and H. Ullmaier, “Magnetic behavior of type-II superconductors with small Ginzburg-Landau parameters,” *Phys. Rev. B* **7**, 136–145 (1973).
- <sup>129</sup>C. Varmazis and M. Strongin, “Inductive transition of niobium and tantalum in the 10-MHz range. I. zero-field superconducting penetration depth,” *Phys. Rev. B* **10**, 1885–1895 (1974).
- <sup>130</sup>R. J. Donnelly, “Cryogenics,” in *Physics Vade Mecum*, edited by H. L. Anderson (American Institute of Physics, New York, 1981) pp. 118–133.
- <sup>131</sup>H. W. Weber, E. Seidl, C. Laa, E. Schachinger, M. Prohammer, A. Junod, and D. Eckert, “Anisotropy effects in superconducting niobium,” *Phys. Rev. B* **44**, 7585–7600 (1991).
- <sup>132</sup>K. S. Wood and D. van Vechten, “Superconducting detectors for photon and particle spectroscopy: Criteria for transitions to normal state,” *Nucl. Instrum. Methods Phys. Res., Sect. A* **314**, 86–112 (1992).
- <sup>133</sup>M. Dressel, “Electrodynamics of metallic superconductors,” *Adv. Condens. Matter Phys.* **2013**, 104379 (2013).
- <sup>134</sup>G. P. Felcher, R. T. Kampwirth, K. E. Gray, and R. Felici, “Polarized-neutron reflections: A new technique used to measure the magnetic field penetration depth in superconducting niobium,” *Phys. Rev. Lett.* **52**, 1539–1542 (1984).
- <sup>135</sup>D. A. Korneev, L. P. Chernenko, A. V. Petrenko, N. I. Balalykin, and A. V. Skripnik, “Measurement of magnetic-field depth profile in superconducting niobium film by polarized neutron reflectometry,” in *Neutron Optical Devices and Applications*, Proceedings of SPIE, Vol. 1738, edited by C. F. Majkrzak and J. L. Wood (SPIE, Bellingham, 1992).
- <sup>136</sup>D. H. Kim, K. E. Gray, J. D. Hettinger, J. H. Kang, and S. S. Choi, “Resistive measurement of the temperature dependence of the penetration depth of Nb in Nb/AlO<sub>x</sub>/Nb Josephson junctions,” *J. Appl. Phys.* **75**, 8163–8167 (1994).
- <sup>137</sup>A. F. Mayadas, R. B. Laibowitz, and J. J. Cuomo, “Electrical characteristics of rf-sputtered single-crystal niobium films,” *J. Appl. Phys.* **43**, 1287–1289 (1972).
- <sup>138</sup>A. Canizo-Cabrera, E. Gómez-Barojas, C. Tabares-Muñoz, R. S. Va-González, and V. García-Vázquez, “Figures of merit for niobium thin films grown on sapphire substrate,” *Mod. Phys. Lett. B* **15**, 639–642 (2001).
- <sup>139</sup>P. R. Broussard, “Parallel critical field in thin niobium films: Comparison to theory,” *J. Low Temp. Phys.* **189**, 108–119 (2017).
- <sup>140</sup>J. Butterworth, “Nuclear magnetic relaxation in niobium metal,” *Proc. Phys. Soc.* **85**, 735–741 (1965).
- <sup>141</sup>F. Ohsumi, K. Matsuta, M. Mihara, T. Onishi, T. Miyake, M. Sasaki, K. Sato, C. Ha, A. Morishita, T. Fujio, Y. Kobayashi, M. Fukuda, and T. Minamisono, “Lattice locations of  $^8\text{Li}$  in Cu,” *Hyperfine Interact.* **120**, 419–422 (1999).
- <sup>142</sup>Z. Salman, A. I. Mansour, K. H. Chow, M. Beaudoin, I. Fan, J. Jung, T. A. Keeler, R. F. Kiefl, C. D. P. Levy, R. C. Ma, G. D. Morris, T. J. Parolin, D. Wang, and W. A. MacFarlane, “ $\beta$ -NMR of isolated  $^8\text{Li}^+$  implanted into a thin copper film,” *Phys. Rev. B* **75**, 073405 (2007).
- <sup>143</sup>Y. Yafet, R. W. Keyes, and E. N. Adams, “Hydrogen atom in a strong magnetic field,” *J. Phys. Chem. Solids* **1**, 137–142 (1956).
- <sup>144</sup>M. I. Dyakonov, A. L. Efros, and D. L. Mitchell, “Magnetic freeze-out of electrons in extrinsic semiconductors,” *Phys. Rev.* **180**, 813–818 (1969).
- <sup>145</sup>V. G. Storchak, D. G. Eshchenko, J. H. Brewer, B. Hitti, R. L. Lichti, and B. A. Aronson, “Magnetic freezeout of electrons into muonium atoms in GaAs,” *Phys. Rev. B* **71**, 113202 (2005).
- <sup>146</sup>K. Ishida, Y. Niino, G.-Q. Zheng, Y. Kitaoka, K. Asayama, and T. Ohtani, “ $^{93}\text{Nb}$  NQR study in layered superconducting  $2H\text{-NbSe}_2$ ,” *J. Phys. Soc. Jpn.* **65**, 2341–2342 (1996).
- <sup>147</sup>R. J. Noer, “Nuclear magnetic relaxation in Nb—Mo alloys,” *Proc. Phys. Soc.* **86**, 309–313 (1965).
- <sup>148</sup>F. Y. Fradin and B. C. Huguélet, “Low temperature  $^{93}\text{Nb}$  nuclear spin-lattice relaxation in Nb and Nb—Mo alloys,” *Phys. Lett. A* **51**, 269–270 (1975).
- <sup>149</sup>E. Thoeng, R. M. L. McFadden, S. Saminathan, G. D. Morris, P. Kolb, B. Matheson, M. Asaduzzaman, R. Baartman, S. R. Dunsiger, D. Fujimoto, T. Junginger, V. L. Karner, S. Kiy, R. Li, M. Stachura, J. O. Ticknor, R. F. Kiefl, W. A. MacFarlane, and R. E. Laxdal, “A new high parallel-field spectrometer at TRIUMF’s  $\beta$ -NMR facility,” *Rev. Sci. Instrum.* **94**, 023305 (2023).
- <sup>150</sup>SRF Nb is typically formed from polished material made of bulk ingots. Similarly, films used in SRF applications are not deposited on ultra-flat substrates.
- <sup>151</sup>M. Lindstrom, B. Wetton, and R. Kiefl, “Modelling the effects of surface roughness on superconductors,” *Phys. Proc.* **30**, 249–253 (2012).
- <sup>152</sup>M. Lindstrom, B. Wetton, and R. Kiefl, “Mathematical modelling of the effect of surface roughness on magnetic field profiles in type II superconductors,” *J. Eng. Math.* **85**, 149–177 (2014).
- <sup>153</sup>M. Lindstrom, A. C. Y. Fang, and R. F. Kiefl, “Effect of surface roughness on the magnetic field profile in the meissner state of a superconductor,” *J. Supercond. Novel Magn.* **29**, 1499–1507 (2016).
- <sup>154</sup>Y. S. Barash, “The magnetic penetration depth influenced by the proximity to the surface,” *J. Phys.: Condens. Matter* **26**, 045702 (2014).
- <sup>155</sup>V. Ngampruetikorn and J. A. Sauls, “Effect of inhomogeneous surface disorder on the superheating field of superconducting RF cavities,” *Phys. Rev. Res.* **1**, 012015(R) (2019).

- <sup>156</sup>E. M. Lechner, J. W. Angle, F. A. Stevie, M. J. Kelley, C. E. Reece, and A. D. Palczewski, "RF surface resistance tuning of superconducting niobium via thermal diffusion of native oxide," *Appl. Phys. Lett.* **119**, 082601 (2021).
- <sup>157</sup>T. Junginger, W. Wasserman, and R. E. Laxdal, "Superheating in coated niobium," *Supercond. Sci. Technol.* **30**, 125012 (2017).
- <sup>158</sup>T. Junginger, S. H. Abidi, R. D. Maffett, T. Buck, M. H. Dehn, S. Gheidi, R. Kiefl, P. Kolb, D. Storey, E. Thoeng, W. Wasserman, and R. E. Laxdal, "Field of first magnetic flux entry and pinning strength of superconductors for rf application measured with muon spin rotation," *Phys. Rev. Accel. Beams* **21**, 032002 (2018).
- <sup>159</sup>L. C. Hebel and C. P. Slichter, "Nuclear spin relaxation in normal and superconducting aluminum," *Phys. Rev.* **113**, 1504–1519 (1959).
- <sup>160</sup>A. Chatzichristos, R. M. L. McFadden, V. L. Karner, D. L. Cortie, C. D. P. Levy, W. A. MacFarlane, G. D. Morris, M. R. Pearson, Z. Salman, and R. F. Kiefl, "Determination of the nature of fluctuations using  $^8\text{Li}$  and  $^9\text{Li}$   $\beta$ -NMR and spin-lattice relaxation," *Phys. Rev. B* **96**, 014307 (2017).
- <sup>161</sup>R. Piessens, E. de Doncker-Kapenga, C. W. Überhuber, and D. K. Kahaner, *QUADPACK: A Subroutine Package for Automatic Integration*, Springer Series in Computational Mathematics, Vol. 1 (Springer, Berlin, 1983).